NASA TECHNICAL NOTE

NASA TN D-5754

c. 1

NASA TN D-5754

FLOW-FIELD INVESTIGATION FOR LARGE-ANGLE CONES WITH SHORT SPIKES AT A MACH NUMBER OF 9.6

by W. Frank Staylor

Langley Research Center
Langley Station, Hampton, Va.

NATIONAL AERONAUTICS AND SPACE ADMINISTRATION • WASHINGTON, D. C. • APRIL 1970

1. Report No. NASA TN D-5754	2. Government Accession No.	3. Recipi
4. Title and Subtitle FLOW-FIELD INVESTIGATION FOR LARGE-ANGLE CONES WITH SHORT SPIKES AT A MACH NUMBER OF 9.6		5. Report Date April 1970 6. Performing Organization Code
7. Author(s) W. Frank Staylor		8. Performing Organization Report No. L-6317
9. Performing Organization Name and Address NASA Langley Research Center Hampton, Va. 23365		10. Work Unit No. 124-64-04-02-23 11. Contract or Grant No.
12. Sponsoring Agency Name and Address National Aeronautics and Space Administration Washington, D.C. 20546		13. Type of Report and Period Covered Technical Note 14. Sponsoring Agency Code
15. Supplementary Notes		

16. Abstract

Tests were conducted with the models at zero angle of attack at a Mach number of 9.6. The test Reynolds numbers based on model diameter ranged from 6×10^4 to 23×10^4 and the model boundary layers were laminar for all tests. The parameter l/δ, the ratio of the spike-cylinder length to the bow-shock standoff distance at the stagnation point, determined the flow stability and the distributions of pressure and heating in the vicinity of the spike. For $l/\delta \leq 0.7$, the flow was detached from the spike tip and steady; for $1.1 \leq l/\delta \leq 2.2$, the flow was attached and steady; and for all other values of l/δ tested, $(l/\delta)_{max} \approx 4$, the flow was unsteady. Heat-transfer measurements on the unspiked models were in good agreement with laminar predictions, and both the spiked and unspiked heating distributions were independent of Reynolds number. The total integrated heating increased with spike length and for steady, attached flow ranged from about 1.1 to 1.3 times the unspiked value. A semi-empirical method is presented that predicted the heating distributions for attached spike flow.

17. Key Words (Suggested by Author(s))
Spikes
Conical flow fields
Heat transfer
Hypersonic laminar flow

18. Distribution Statement
Unclassified – Unlimited

19. Security Classif. (of this report)	20. Security Classif. (of this page)	21. No. of Pages	22. Price*
Unclassified	Unclassified	37	$3.00

*For sale by the Clearinghouse for Federal Scientific and Technical Information
Springfield, Virginia 22151

FLOW-FIELD INVESTIGATION FOR LARGE-ANGLE CONES WITH SHORT SPIKES AT A MACH NUMBER OF 9.6

By W. Frank Staylor
Langley Research Center

SUMMARY

Heat-transfer and schlieren data were obtained for four large-angle, sharp and blunt cones with spikes of various lengths located at the apex. Tests were conducted with the models at zero angle of attack at a Mach number of 9.6. The test Reynolds numbers based on model diameter ranged from 6×10^4 to 23×10^4 and the model boundary layers were laminar for all tests.

The parameter l/δ, the ratio of the spike-cylinder length to the bow-shock standoff distance at the stagnation point, determined the flow stability and the distributions of pressure and heating in the vicinity of the spike. For $l/\delta \leqq 0.7$, the flow was detached from the spike tip and steady; for $1.1 \leqq l/\delta \leqq 2.2$, the flow was attached and steady; and for all other values of l/δ tested, $(l/\delta)_{max} \approx 4$, the flow was unsteady. Heat-transfer measurements on the unspiked models were in good agreement with laminar predictions, and both the spiked and unspiked heating distributions were independent of Reynolds number. The total integrated heating increased with spike length and for steady, attached flow ranged from about 1.1 to 1.3 times the unspiked value. A semiempirical method is presented that predicted the heating distributions for attached spike flow.

INTRODUCTION

Previous investigations, such as references 1 to 9, have shown that long protruding spikes can significantly change the drag, lift, and heating on a blunt body. For several recently proposed applications, it is desired to introduce a gas sampling probe which will not substantially alter the body drag. One such proposal is to use a short, instrumented probe extended just beyond the bow shock into the free-stream flow ahead of an entry vehicle. The instrumented probe could collect gas samples uncontaminated by ablation products from the body heat-protection system; these samples could be analyzed to determine the gas composition, density, pressure, and temperature profiles during planetary entry.

The present investigation was initiated to study the effects that short, small diameter spikes located in the vicinity of the bow shock would have upon the flow fields of high-drag, conical bodies such as those of references 1, 10, and 11. Spike-induced flow oscillations observed by previous investigators (refs. 1, 5, 6, 9, and 12, for instance) were of particular interest in that such phenomena could have undesirable effects upon both the structure and instrumentation of an entry vehicle. Spikes of various lengths were tested at the apex of four large-angle, sharp and blunted cones at zero angle of attack and at a free-stream Mach number of 9.6. Both heat-transfer distributions and schlieren photographs were obtained.

SYMBOLS

D_n cone-nose diameter

D_b cone-base diameter

h heat-transfer coefficient

H integrated heat-transfer coefficient, $2\pi \int hr\, ds$

k thermal conductivity

l spike-cylinder length measured from stagnation point (fig. 1)

l' spike-cylinder length measured from cone virtual apex (fig. 18)

M free-stream Mach number

p local cone-surface static pressure

$p_{t,1}$ tunnel stagnation pressure

$p_{t,2}$ stagnation pressure behind normal shock

r local radius measured from cone center line

R_D free-stream Reynolds number based on model diameter

s surface distance

t	time measured from flow initiation
t_{pc}	time at phase change
t'	effective tunnel flow delay time
T_{aw}	adiabatic wall temperature
T_i	initial model temperature
T_{pc}	phase change temperature
$T_{t,1}$	tunnel stagnation temperature
$\overline{T}$	temperature parameter, $\frac{T_{pc} - T_i}{T_{aw} - T_i}$
v	velocity
x	axial distance from cone stagnation point
α	thermal diffusivity
β	heat-transfer parameter, $\frac{h\sqrt{\alpha t_{pc}}}{k}$
δ	bow-shock standoff distance measured from stagnation point $l = r = 0$
δ'	bow-shock standoff distance measured from cone virtual apex $l = r = 0$ (fig. 18)
θ	conical shock wave half-angle (fig. 15)
μ	viscosity
ρ	density
σ	vortex cone half-angle (fig. 15)
ϕ	model cone half-angle

Subscripts:

a	flow attachment
o	stagnation point, $r = 0$
s	flow separation
∞	tunnel steady-flow conditions

APPARATUS AND TESTS

Models

Sketches of the cone models and spike employed in the present investigation are shown in figure 1. The four models were constructed from fiber-glass-reinforced plastic formed on a knurled sleeve and were doweled to a support sting. The models had sharp shoulders and the base diameters D_b were 5.0 cm. Provision was made at the model apex for the installation of a 0.56-mm-diameter spike that was doweled at various positions along the model axis. The spike had a sharp conical tip with a half-angle of 40°. The thin metallic strip attached to the model shank was used to detect flow initiation ($t = 0$).

Apparatus and Test Methods

The tests were conducted in the Langley 11-inch hypersonic tunnel, described in references 13 and 14. For the present tests the Mach number 9.6 nozzle was employed and the models were alined with the flow at zero angle of attack. A quick-opening valve allowed the tunnel stagnation pressure $p_{t,1}$ to reach its steady value at about $t = 0.5$ second. Although a preliminary preheating procedure was used, the tunnel stagnation temperature $T_{t,1}$ did not obtain its steady value until $t = 2$ to 3 seconds.

A sketch of the model and equipment arrangement for the phase-change-coating heat-transfer tests (ref. 15) is shown in figure 2. The phase coatings were sprayed on the front surface of the models to depths less than 0.05 mm and had a phase-change temperature T_{pc} of 478° K. The model was positioned somewhat aft of the window center line so that the model surface ray nearest to the camera could be photographed at a near-perpendicular angle. A 16-mm motion-picture camera was used to photograph the phase-change history at a nominal film speed of 8 frames per second. Both the motion-picture camera and light sources were actuated at about $t = -3$ seconds which allowed sufficient time for the camera to accelerate to its calibrated speed and yet prevented the light sources from heating the models excessively before flow initiation.

Heat-transfer tests were conducted on all four models with four spike lengths l at a nominal free-stream Reynolds number of $R_{D,\infty} = 6 \times 10^4$. Tests were also made on two models $\left(\frac{D_n}{D_b} = 0.25 \text{ and } 0.50 \quad \text{with} \quad \phi = 60^o\right)$ with spike lengths of $\frac{l}{D_b} = 0$ and 0.0767 at nominal Reynolds numbers of 11×10^4 and 16×10^4.

For the schlieren tests, the model was positioned near the window center line and schlieren photographs were obtained with a still camera illuminated by a short-duration high-intensity light source. Four or five schlieren photographs were taken during each run at intervals of about 3 seconds. The tunnel stagnation temperature and pressure were measured and recorded by fast-response instruments during both the heat-transfer and schlieren tests.

Schlieren tests were conducted on two models, $\frac{D_n}{D_b} = 0.25$ and 0.50, $\phi = 60^o$, with various spike lengths at nominal Reynolds numbers of 6×10^4, 11×10^4, and 23×10^4. The quality of the schlieren photographs taken at the lower Reynolds numbers was poor; hence, only the photographs for $R_{D,\infty} = 23 \times 10^4$ are shown.

Heat-Transfer Measurements

In figure 3 typical photographs are shown of the recession history of the phase-change coatings for an unspiked and a spiked configuration. The theory and technique for determining heat-transfer coefficients h from such recession histories are given in reference 15. In order to evaluate absolute values of h on a model, it is necessary to determine the model material parameter $\sqrt{\alpha}/k$. However, heat-transfer distributions can be evaluated without knowledge of this parameter if all values are related to a model reference point. For the present tests the model stagnation point ($r = 0$) was used as the reference point and the ratio of the local heating to stagnation-point heating can be expressed as

$$\frac{h}{h_o} = \sqrt{\frac{t_{pc,o}}{t_{pc}}}$$

when it is assumed that $\beta = \beta_o$.

In order to correct for the erroneous heating rates encountered during the tunnel starting procedure (fig. 4(a)), an effective tunnel flow delay time t' is induced into the equation

$$\frac{h}{h_o} = \sqrt{\frac{t_{pc,o} - t'}{t_{pc} - t'}}$$

Although the heat-transfer values on most of the model's surface would not be affected if a delay time of 1.0 second were neglected in the present tests, large errors would occur in regions of high heating (that is, t_{pc} small). Since these values are of primary interest, it was necessary to evaluate t'.

For instantaneous tunnel flow, $t' = 0$, t_{pc} is proportional to the parameter $\beta_\infty^2/R_{D,\infty}$, and therefore, at any given point on a model with a laminar boundary layer, h_∞^2 is proportional to $R_{D,\infty}$. Typical profile histories of the stagnation pressure and temperature are sketched in figure 4(a) for $t_\infty = 2$ and 3 seconds, and the resulting histories of the parameter $\left(R_D/R_{D,\infty}\right)\left(\beta_\infty/\beta\right)^2$ are given in figure 4(b). The reference temperature parameter $\overline{T}$, and hence β (from ref. 15), was determined by assuming that the adiabatic wall temperature T_{aw} on the blunt models was equal to the instantaneous tunnel stagnation temperature (ref. 16) and $T_i = 295^\circ$ K.

Theoretical heating profiles h/h_o were calculated for the four models by using the flow-field predictions of reference 17 and the heating equations of reference 18. Values of t' were determined for the unspiked configurations ($l = 0$) by matching the experimental heating profiles with the theoretical values in the stagnation region $\left(\frac{r}{D_b} = 0 \text{ to } 0.10\right)$. These t' values are presented in figure 4(c) as a function of the time delay parameter $\int_0^{t_\infty}\left[1 - \left(\frac{R_D}{R_{D,\infty}}\right)\left(\frac{\beta_\infty}{\beta}\right)^2\right]dt$. All values of t' were correlated within a 1/8-second band which is the expected accuracy of the initial flow detection for a nominal film speed of 8 frames per second. In all subsequent data presentations, the faired solid line was used to evaluate t' for both spiked and unspiked configurations.

RESULTS AND DISCUSSION

Schlieren Data

Photographs.- Typical schlieren photographs are presented in figures 5(a) and 5(b) for two models, $\frac{D_n}{D_b} = 0.25$ and 0.50, respectively, $\phi = 60^\circ$, with various spike lengths. In figure 5(a) the left photograph shows a steady detached bow shock ($l = 0$) and the center and right photographs show shocks attached to the spike tip that are unsteady. (The center and right photographs were taken only a few seconds apart during the same test run, $\frac{l}{D_b} = 0.132$.) In figure 5(b) the left photograph shows a steady detached bow shock, the center an unsteady detached bow shock, and the right a steady shock attached to the spike tip. (The center and right photographs were scribed to aid in identification of the spike and bow shocks.)

Bow-shock characteristics.- Bow-shock shapes measured from the schlieren photographs of two unspiked models, $\frac{D_n}{D_b} = 0.25$ and 0.50, $\phi = 60^\circ$, are presented in figures 6(a) and 6(b), respectively, and are compared with theoretical shock shapes of reference 17. The measured and theoretical shock shapes are generally in good agreement. Schlieren photographs were not obtained for the two pointed models, $\frac{D_n}{D_b} = 0.0$, $\phi = 60^\circ$ and $\phi = 70^\circ$, but their theoretical shock shapes are given in figure 6(c). In figure 7 measured bow-shock standoff distances at the stagnation point for the present data and that of references 1 and 10 are presented as a function of Mach number and are compared with the theoretical values of reference 17. The present data are about $0.003D_b$ above the theoretical values which is probably caused by the inability of the theory to account for either boundary-layer or shock thickness.

Flow stability.- The schlieren photographs of figure 5 illustrated the four types of flow that can occur when spikes of varying lengths protrude from a large-angle cone, namely – steady, detached; unsteady, detached; steady, attached; and unsteady, attached. In reference 1 these four types of flow were detected and were found to be a function of the parameter l/δ. In figure 8, l/δ is plotted against l/D_b for all the present data ($M = 9.6$, $\phi = 60^\circ$) and for those of reference 1 ($M = 3.0$ to 6.0, $\phi = 60^\circ$). It can be seen that all the present data are in agreement with the l/δ boundaries established in reference 1 for the four types of flow.

Spike-length requirements for both detached and attached steady flows are presented in figure 9 as a function of Mach number for $\phi = 60^\circ$. These curves were calculated by using flow criteria from figure 8 ($l/\delta \leq 0.7$ for the steady detached-flow boundary and $1.1 \leq l/\delta \leq 2.2$ for the steady attached-flow boundaries) with the predicted δ/D_b values from reference 17. (See fig. 7.) In figure 9(b) it is seen that steady attached flow (hatched region) can be maintained over a large Mach number range for a single spike length. For instance, steady flows can be maintained from $M = 6$ to $M = 20$ for $\frac{l}{D_b} = 0.02$, $\frac{D_n}{D_b} = 0$, and from $M = 3.5$ to $M = 20$ for $\frac{l}{D_b} = 0.09$, $\frac{D_n}{D_b} = 0.50$. In general, this Mach number range increases with cone bluntness, nose diameter, and probably with cone angle. (Data substantiating the last statement are not available.)

Heat Transfer

Unspiked models, $l = 0$.- Heat-transfer distribution data are presented in figure 10 for the two $\phi = 60^\circ$ blunt cone models at three values of $R_{D,\infty}$. The distributions h/h_o are in good agreement with theoretical laminar values calculated from references 17 and 18 and are essentially independent of $R_{D,\infty}$. This agreement was forced in the

stagnation region by the determination of the value of t'. In figure 11 heat-transfer distribution data are given for the four sharp and blunt cone models at $R_{D,\infty} \approx 6 \times 10^4$. Again, all data are in good agreement with the theoretical calculations.

Spiked models, $l > 0$.- Heat-transfer distribution data are presented in figure 12 for the two $\phi = 60^\circ$ blunt cone models with $l/D_b = 0.0767$ at three values of $R_{D,\infty}$. The distributions are essentially independent of $R_{D,\infty}$ and show no indications of transition to turbulent flow. In figure 13 heat-transfer distribution data are given for all four models with various spike lengths at $R_{D,\infty} \approx 6 \times 10^4$. The unspiked data ($l = 0$) distributions from figure 11 are shown for comparison and indications of whether the flow was attached or detached from the spike tip (determined from fig. 8) are denoted in the symbol key. For all detached tip flows the heating values were very similar to those of the unspiked models from $\frac{r}{D_b} = 0.05$ to $\frac{r}{D_b} = 0.50$. The heating distributions for attached tip flows were a strong function of the spike length but approached the unspiked values downstream of peak heating.

Heating at flow attachment to the cone h_a, extrapolated heating at the base of the spike $h_{r=0}$, and the integrated heating on the entire model surface H are presented in figures 14(a), 14(b), and 14(c), respectively, as a function of spike length. The flow types are indicated by solid or dashed lines and plain or flagged symbols. Peak heating occurred at flow attachment and for attached spike flows the general level of these values were about $\frac{h_a}{h_o} = 1.0$ for blunted cones and $\frac{h_a}{h_o} = 0.7$ for pointed cones. At the base of the spike, $r \approx 0$, the extrapolated heating values decrease with increasing spike length $\left(h_{r=0} \to 0;\ l \to \infty\right)$ and approached the stagnation value for decreasing spike length $\left(\frac{h_{r=0}}{h_o} \to 1.0;\ l \to 0\right)$. The increase of integrated heating was small (<10 percent) for detached spike flows, but increased with l for attached spike flows and a maximum value of $\frac{H}{H_{l=0}} = 1.5$ was obtained for the present tests. However, for steady attached spike flows, the integrated heating ranged between values of $\frac{H}{H_{l=0}} = 1.1$ to $\frac{H}{H_{l=0}} = 1.3$.

Flow Analysis

A postulated flow model is presented in figure 15 which illustrates the flow phenomena that is believed to occur in the vicinity of large-angle spiked cones. This model is based upon observations of schlieren and pressure data of reference 1 (see fig. 12 of ref. 1) and the schlieren and heat-transfer data of the present paper. The flow attaches to the spike tip and forms a conical shock wave of half-angle θ as though attached to the tip of a smaller cone of half-angle σ ($\sigma < \phi$). This smaller cone is a separated vortex

that flows along the model surface from its attachment point at r_a toward the spike tip. It is believed that a smaller secondary vortex exists in the vicinity of the spike base. At the intersection of the conical and bow shock waves, a third shock wave occurs which is nearly normal to the conical spike flow. This flow exhausts on to the model surface and mixes with flow passing through the bow shock as both accelerate toward the model shoulder.

Measured values of θ (plain symbols) are presented in figure 16 as a function of l/δ. Corresponding values of σ (flagged symbols) were determined from conical shock charts (ref. 19) and are also shown in figure 16. These data are in good agreement with the linear equation for σ in degrees:

$$\sigma = 60 - 5\,\frac{l}{\delta} \tag{1}$$

Static pressures p_s in the separated vortex region were calculated by using equation (1) with the conical shock charts and are presented in figure 17 as a function of l/δ for Mach numbers of 4.5, 6.0, and 9.6. The separated pressure data from reference 1 $\left(\frac{r}{D_b} = 0.033, \text{ flagged symbols}\right)$ are generally in good agreement with the calculated values which are relatively insensitive to Mach number. The maximum pressures measured on the models are presented at the top of the figure (plain symbols) and should indicate the general level of the pressure at flow attachment p_a. Because of the sparse location of pressure orifices, it is believed that the actual maximum pressures were somewhat greater than any of the measured values $\left(r_{orifice} \neq r_a\right)$. The equation

$$\frac{p_a}{p_{t,2}} = 1.0 + 0.02\,\frac{l}{\delta} \tag{2}$$

which is approximately parallel to the maximum measured values will be used in subsequent calculations. (See fig. 17.)

Flow attachment was assumed to occur at the point of maximum heating which can be obtained accurately from the present heat-transfer data. (See fig. 13.) The flow attachment points r_a are presented in figure 18 as a function of the virtual parameter l'/δ' and are well correlated by the equation

$$\frac{r_a}{D_b} = 0.400 + 0.283\,\frac{l'}{\delta'} \tag{3}$$

Equation (3) applies only for $\phi = 60^\circ$, but the data of figure 16 indicate that it should be applicable at any hypersonic Mach number.

In general, laminar heating can be calculated if the velocity v, density ρ, and viscosity μ distributions along the edge of the boundary layer can be determined. (See ref. 18.) These flow parameters can be calculated from predicted pressure distributions if it is assumed that the flow expands isentropically from a stagnation pressure which is assumed to the maximum pressure on the model p_a. It is also assumed that the stagnation temperature of this flow is equal to $T_{t,1}$. Pressure distribution data from reference 1 are given in figure 19 for various spiked models at $M = 6.0$ and are compared with predicted values. The predicted values were calculated as follows:

(1) At location r_a (eq. (3)), the flow at pressure p_a (eq. (2)) was expanded isentropically toward the spike to a pressure p_s. (See fig. 17.) Figure 17 is obtained by using equation (1) with reference 19.

(2) The flow was expanded so that the velocity gradient dv/dr is constant from r_a to $0.6r_a$.

(3) The flow was also expanded isentropically toward the model shoulder with a velocity gradient equal to that established in step (2) until the pressure intersects the predicted curve from reference 16 for $l = 0$.

(4) Flow-field predictions of reference 16 are applicable from the pressure intersection to the model shoulder, $\frac{r}{D_b} = 0.5$. The sparsity of data, particularly in the vicinity of flow attachment, does not allow the present method to be fully evaluated; however, most of the data are within ±10 percent of the predicted values.

The laminar heating equation

$$h \propto \frac{\rho v k r}{\sqrt{\int_0^s \rho v \mu r^2 \, ds}} \tag{4}$$

from reference 18 was used to calculate the heating distributions where $s = 0$ at r_a for both the vortex $(r \leqq r_a)$ and primary $(r \geqq r_a)$ flows. Isentropic relationships (ref. 19) were used to calculate the ρ, v, and the flow temperature (hence, k and μ) profiles from the pressure distributions. In figure 20 the predicted distributions are compared with the test data for $\frac{D_n}{D_b} = 0.00$, 0.25, and 0.50, $\phi = 60^\circ$, $\frac{l}{D_b} = 0.0767$, and it can be seen that the agreement is generally good.

The data correlations in figures 16, 17, and 18 and the data predictions in figures 19 and 20 indicate that the postulated flow model is basically correct. Although the present

data correlations apply only for $\phi = 60^{\circ}$, it is believed that similar correlations exist for any large-angle cone with a detached bow shock wave.

CONCLUDING REMARKS

Schlieren and heat-transfer data were obtained for four large-angle sharp and blunted cones with spikes of various lengths located at the apex. The tests were conducted at a free-stream Mach number of 9.6 with the models at zero angle of attack. Heat-transfer measurements were obtained by using the phase-change coating method at nominal free-stream Reynolds numbers based on model diameter ranging from 6×10^4 to 16×10^4, and the schlieren tests were conducted at a Reynolds number of 23×10^4.

The present tests confirmed a conclusion drawn in reference 1 that most flow phenomena produced by the spikes were a function of the parameter l/δ, the ratio of the spike-cylinder length to the bow-shock standoff distance at the stagnation point. For $l/\delta \leqq 0.7$, the flow was detached from the spike tip and steady, and for $1.1 \leqq l/\delta \leqq 2.2$, the flow was attached and steady. Unsteady flow occurred for all other values of l/δ tested. The Mach number range over which attached steady-flow conditions can be maintained for a given spike length increased with cone bluntness.

Heat-transfer measurements on the unspiked models were in good agreement with laminar predictions. Both the spiked and unspiked distributions were independent of Reynolds number and the boundary layers were laminar. For detached spike flow, the heating distributions were essentially unchanged from those measured on the unspiked models. For attached spike flow, the maximum heating values were generally less than the unspiked stagnation-point values and occurred at the point of flow attachment to the model. The total integrated heating on the models increased with spike length and for steady attached spike flows ranged from about 1.1 to 1.3 times the unspiked value.

A semiempirical method is presented that predicted the heating distributions on models with attached spike flow. This method is based on a flow model that was found to be consistent with correlations of schlieren, pressure, and heat-transfer data from both the present tests and those of reference 1.

Langley Research Center,
National Aeronautics and Space Administration,
Langley Station, Hampton, Va., February 10, 1970.

REFERENCES

1. McGhee, Robert J.; and Staylor, W. Frank: Aerodynamic Investigation of Sharp Cone-Cylinder Spikes on 120° Blunted Cones at Mach Numbers of 3.00, 4.50, and 6.00. NASA TN D-5201, 1969.

2. Harman, Richard W.; and Boatwright, William B.: Investigation of the Aerodynamic Characteristics of a Reentry Capsule With Various Nose Shapes at a Mach Number of 2.91, Including Studies of Nose Spikes as a Means of Control. NASA TM X-426, 1961.

3. Sims, William H.; and Hahn, Jerry S.: Aerodynamic Drag on Spiked Blunt Bodies in Low-Density Hypersonic Flow. AEDC-TDR-64-160, U.S. Air Force, Aug. 1964.

4. Wagner, Richard D., Jr.; Pine, W. Clint; and Henderson, Arthur, Jr.: Laminar Heat-Transfer and Pressure-Distribution Studies on a Series of Reentry Nose Shapes at a Mach Number of 19.4 in Helium. NASA TN D-891, 1961.

5. Zakkay, Victor: Preliminary Experimental Investigation of the Flow About a Blunt Body With Flow-Separation Spikes at $M_\infty = 7.9$. AFOSR 219, U.S. Air Force, Feb. 1961.

6. Crawford, Davis H.: Investigation of the Flow Over a Spiked-Nose Hemisphere-Cylinder at a Mach Number of 6.8. NASA TN D-118, 1959.

7. Bogdonoff, Seymour M.; and Vas, Irwin E.: Preliminary Investigations of Spiked Bodies at Hypersonic Speeds. J. Aero/Space Sci., vol. 26, no. 2, Feb. 1959, pp. 65-74.

8. Wood, C. J.: Hypersonic Flow Over Spiked Cones. J. Fluid Mech., vol. 12, pt. 4, Apr. 1962, pp. 614-624.

9. Holden, Michael S.: Experimental Studies of Separated Flows at Hypersonic Speeds. Part I: Separated Flows Over Axisymmetric Spiked Bodies. AIAA J., vol. 4, no. 4, Apr. 1966, pp. 591-599.

10. Campbell, James F.; and Howell, Dorothy T.: Supersonic Aerodynamics of Large-Angle Cones. NASA TN D-4719, 1968.

11. Krumins, Maigonis V.: Drag and Stability of Mars Probe/Lander Shapes. J. Spacecraft Rockets, vol. 4, no. 8, Aug. 1967, pp. 1052-1057.

12. Maull, D. J.: Hypersonic Flow Over Axially Symmetric Spiked Bodies. J. Fluid Mech., vol. 8, pt. 4, Aug. 1960, pp. 584-592.

13. Schaefer, William T., Jr.: Characteristics of Major Active Wind Tunnels at the Langley Research Center. NASA TM X-1130, 1965.

14. Bertram, Mitchel H.: Boundary-Layer Displacement Effects in Air at Mach Numbers of 6.8 and 9.6. NASA TR R-22, 1959. (Supersedes NACA TN 4133.)

15. Jones, Robert A.; and Hunt, James L.: Use of Fusible Temperature Indicators for Obtaining Quantitative Aerodynamic Heat-Transfer Data. NASA TR R-230, 1966.

16. Hermach, C. A.; Kraus, Samuel; and Reller, John O., Jr.: Reductions in Temperature-Recovery Factor Associated With Pulsating Flows Generated by Spike-Nosed Cylinders at a Mach Number of 3.50. NACA RM A56L05, 1957.

17. South, Jerry C., Jr.: Calculation of Axisymmetric Supersonic Flow Past Blunt Bodies With Sonic Corners, Including a Program Description and Listing. NASA TN D-4563, 1968.

18. Lees, Lester: Laminar Heat Transfer Over Blunt-Nosed Bodies at Hypersonic Flight Speeds. Jet Propulsion, vol. 26, no. 4, Apr. 1956, pp. 259-269, 274.

19. Ames Research Staff: Equations, Tables, and Charts for Compressible Flow. NACA Rep. 1135, 1953. (Supersedes NACA TN 1428.)

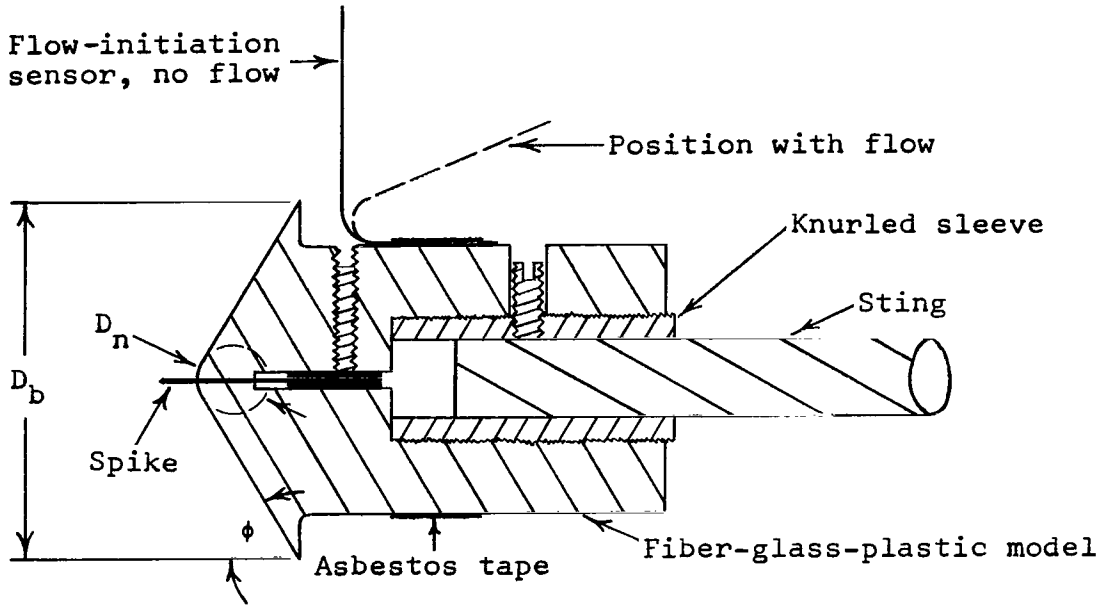

Sketch of models

ϕ, deg	D_n / D_b	ℓ / D_b
70	0	0.0212
60	0	.0489
60	0.25	.0767
60	0.50	.1045

Models tested Spikes tested

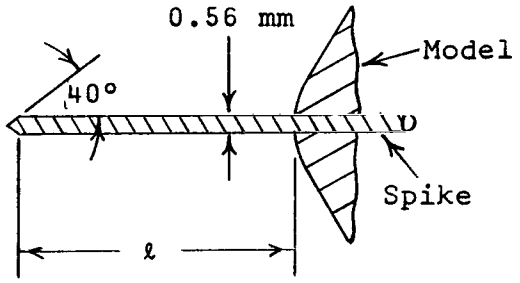

Sketch of spike

Figure 1.- Sketch of models and spike. D_b = 5.0 cm.

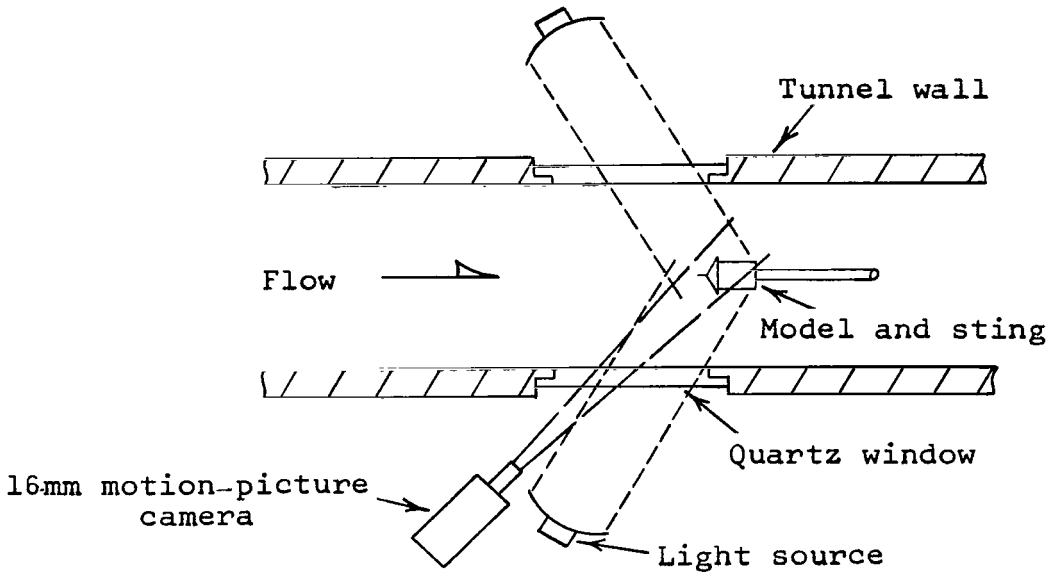

Figure 2.- Model and equipment arrangement for heat-transfer tests.

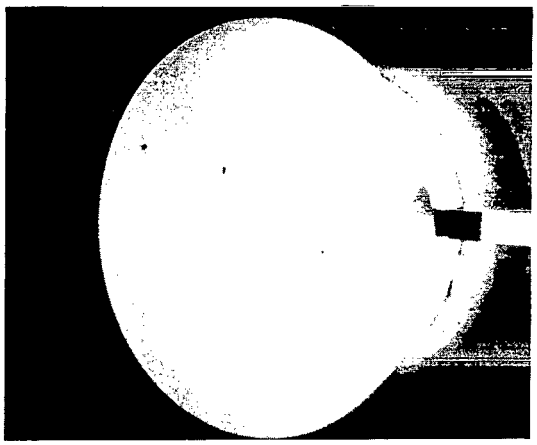

$t < 0$

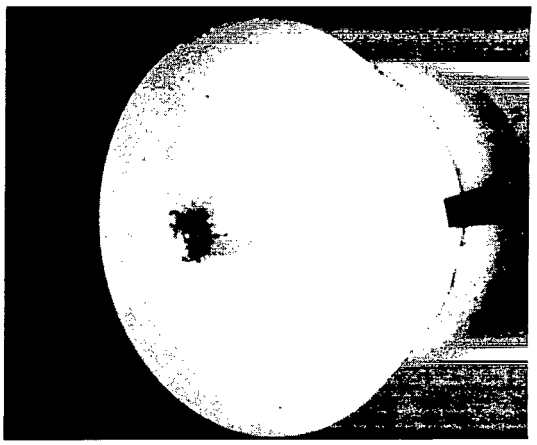

$t = 3.94$

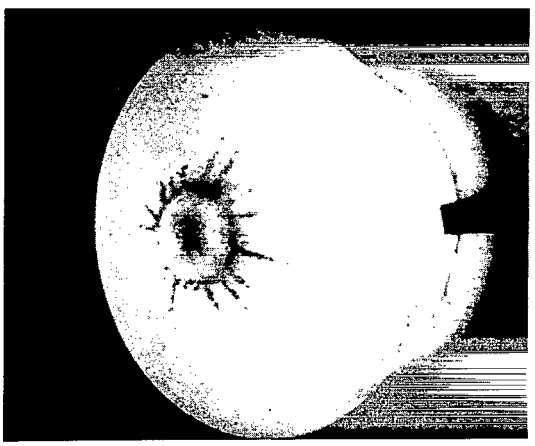

$t = 7.19$

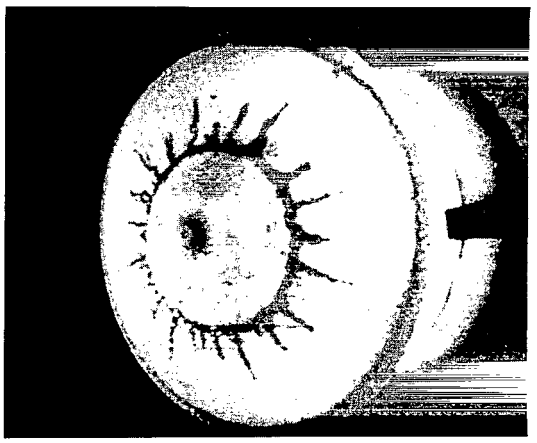

$t = 12.81$

(a) $\frac{l}{D_b} = 0.0000$.

L-70-1522

Figure 3.- Typical photographs of paint recession during tests. $\Phi = 60^0$; $\frac{D_n}{D_b} = 0.25$; $R_{D,\infty} \approx 6 \times 10^4$.

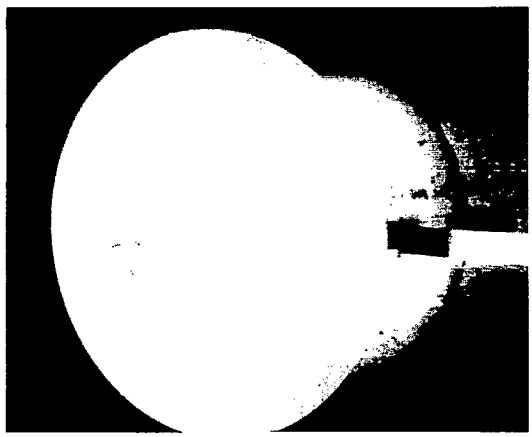

$t < 0$

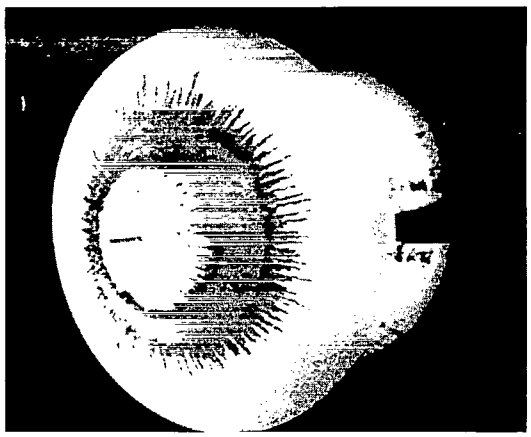

$t = 3.94$

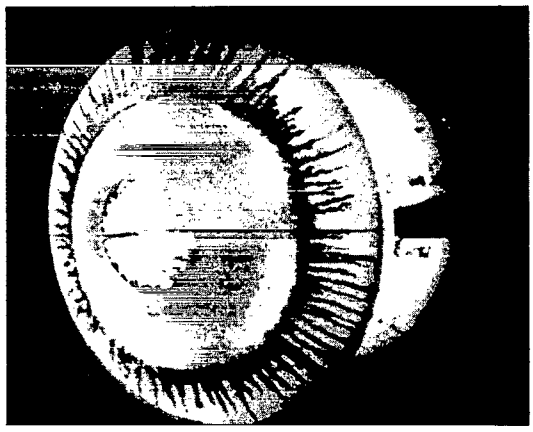

$t = 8.19$

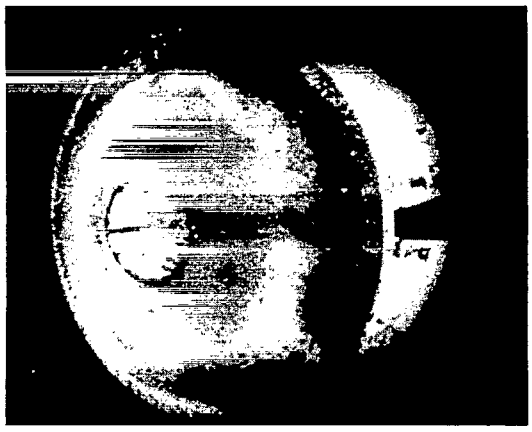

$t = 12.56$

L-70-1523

(b) $\frac{l}{D_b} = 0.1045$.

Figure 3.- Concluded.

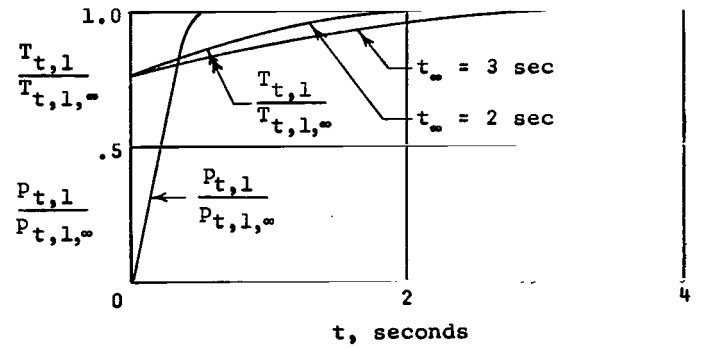

(a) Tunnel flow history.

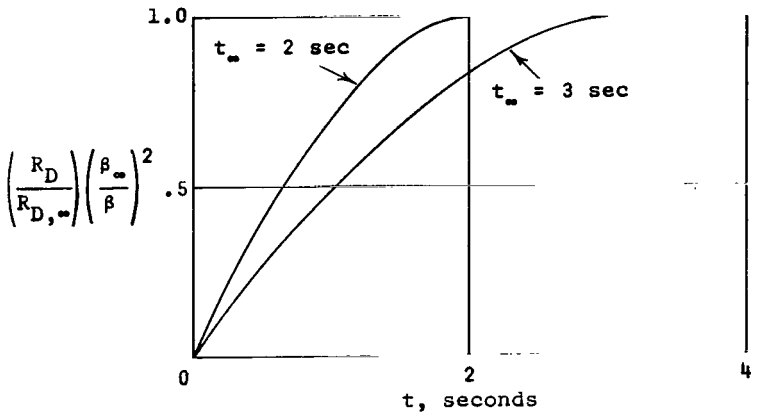

(b) Heating parameter history.

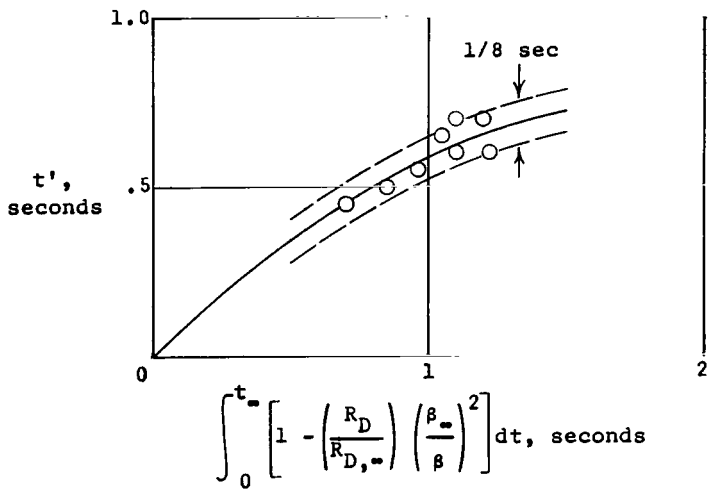

(c) Correlation of t'.

Figure 4.- Empirical evaluation of t'.

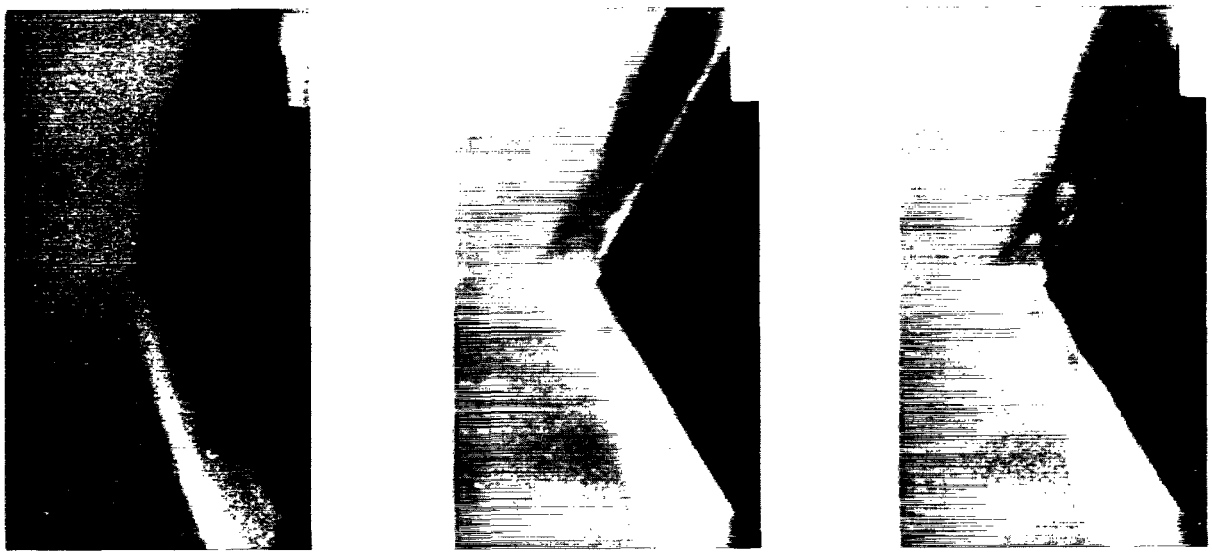

No probe $\quad l/D_b = 0.132 \quad l/D_b = 0.132$

(a) $\frac{D_n}{D_b} = 0.25.$

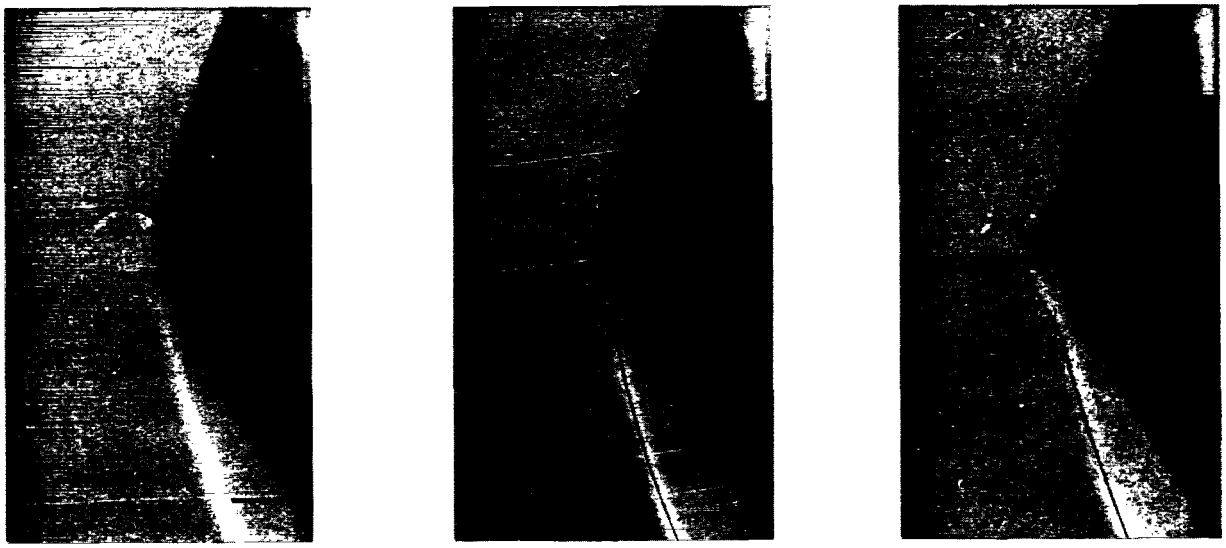

No probe $\quad l/D_b = 0.044 \quad l/D_b = 0.094$

L-70-1524

(b) $\frac{D_n}{D_b} = 0.50.$

Figure 5.- Typical schlieren photographs. $\Phi = 60^0$; $R_{D,\infty} = 23 \times 10^4$.

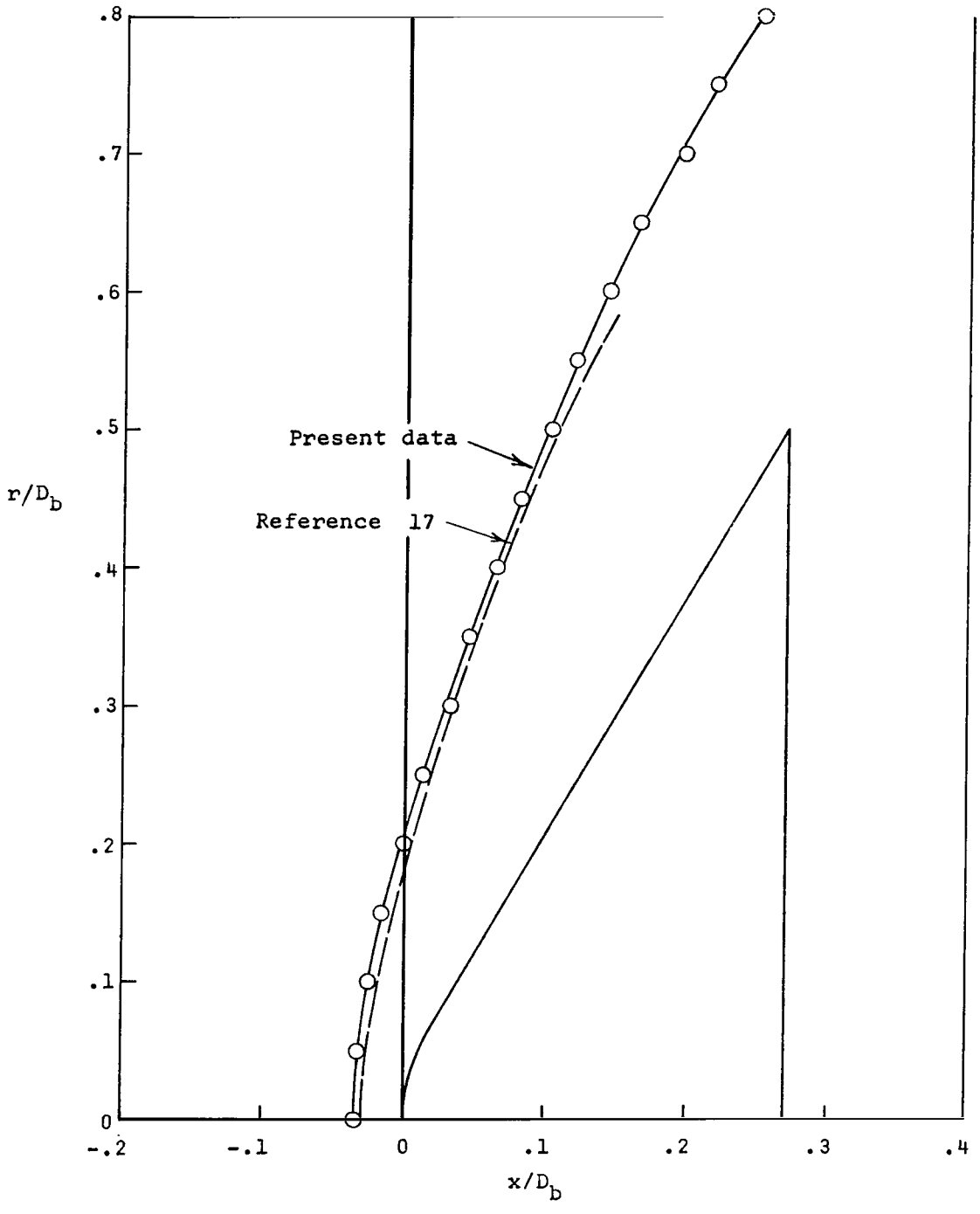

(a) $\frac{D_n}{D_b} = 0.25$; $\Phi = 60^0$.

Figure 6.- Shock shape. $R_{D,\infty} = 23 \times 10^4$.

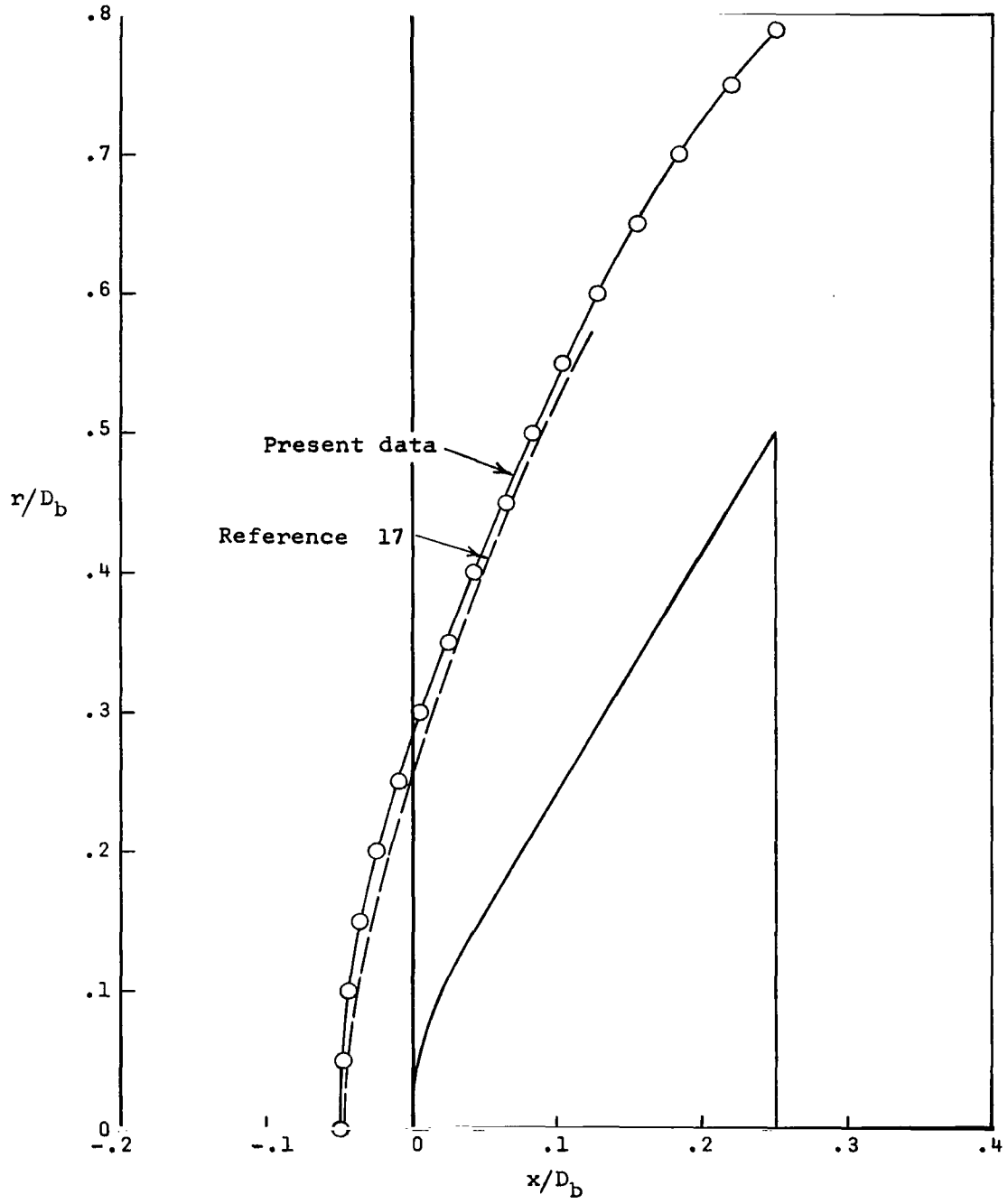

(b) $\frac{D_n}{D_b} = 0.50$; $\Phi = 60^{\circ}$.

Figure 6.- Continued.

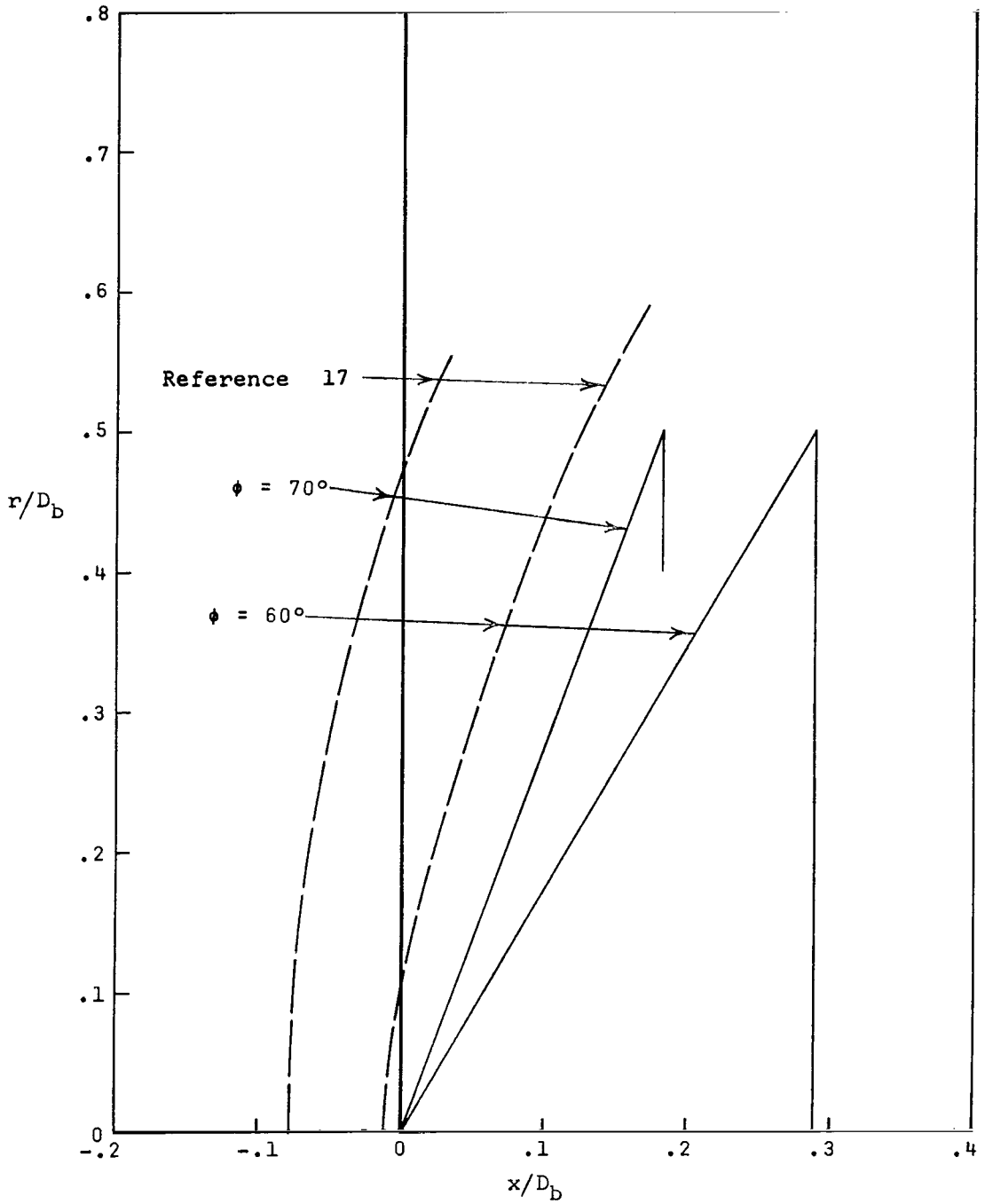

(c) $\frac{D_n}{D_b} = 0.0$; $\Phi = 60^0$ and 70^0.

Figure 6.- Concluded.

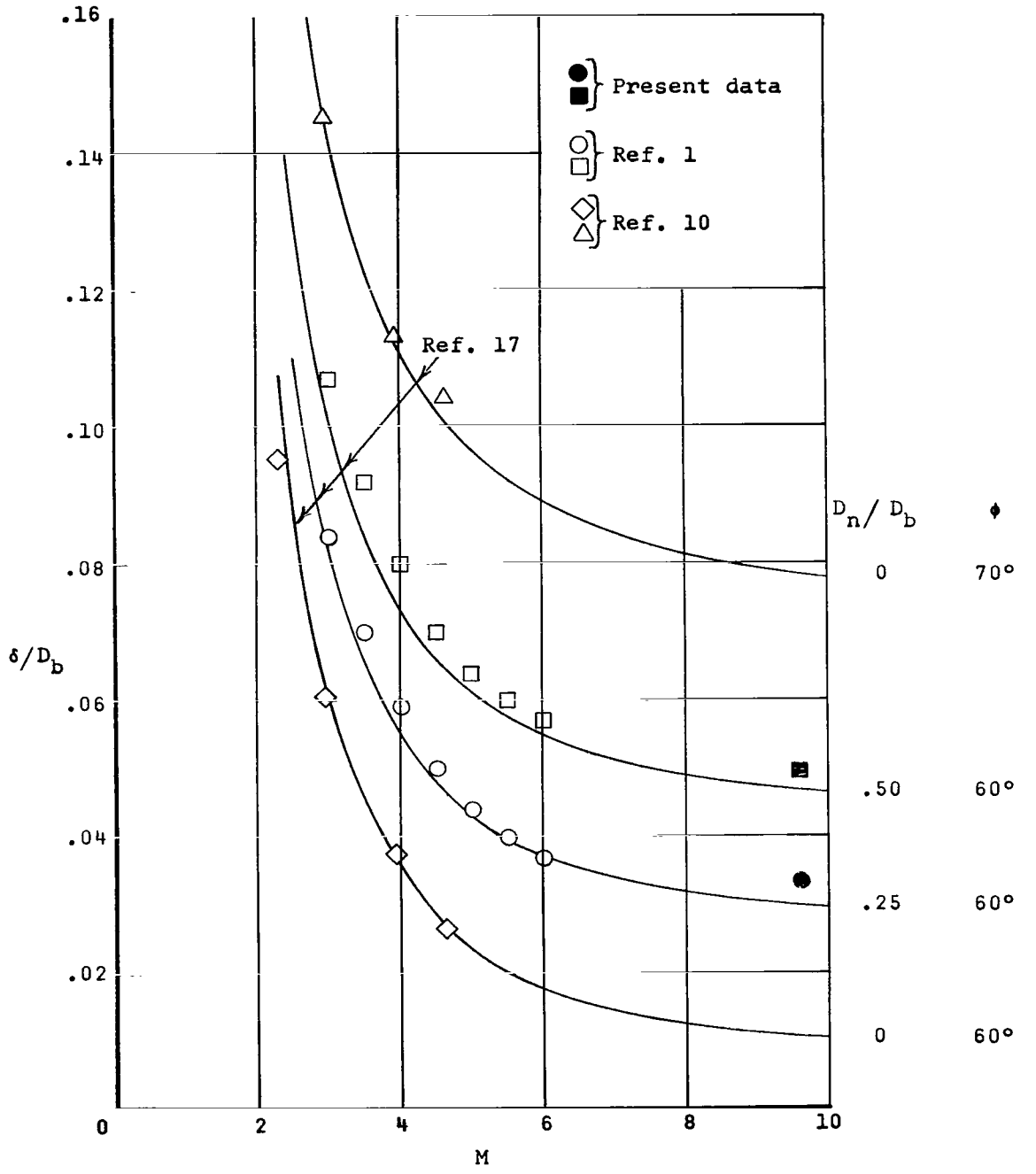

Figure 7.- Bow-shock standoff distance as a function of Mach number. $\ell = 0$.

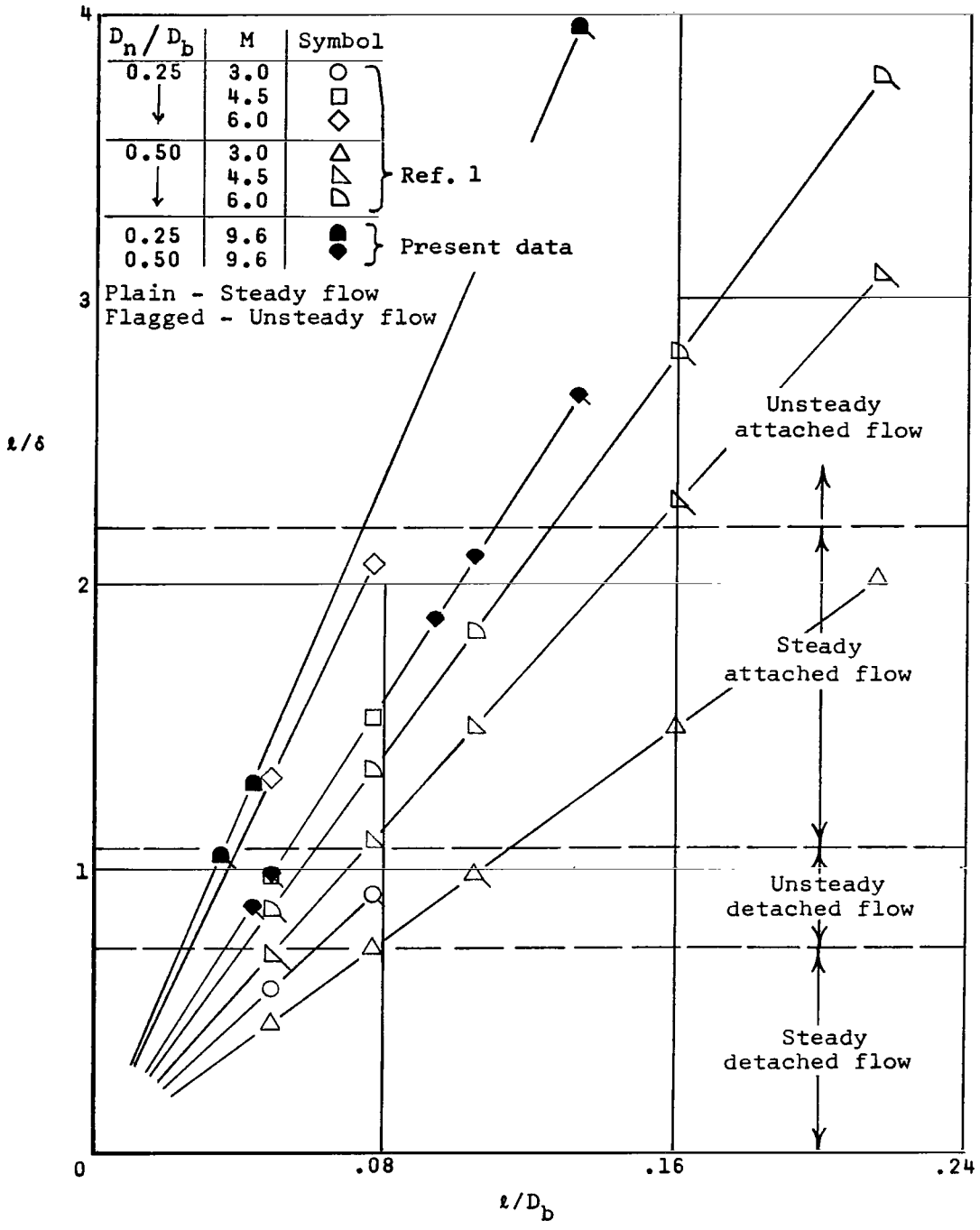

Figure 8.- Bow-shock stability. $\Phi = 60^{0}$.

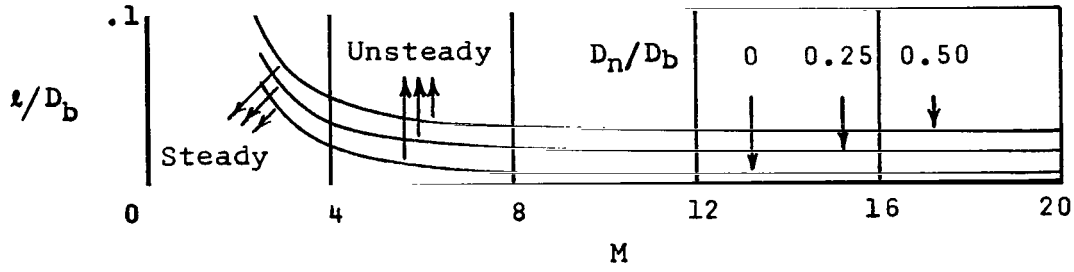

(a) Steady detached flow. $\ell/\delta \leq 0.7$.

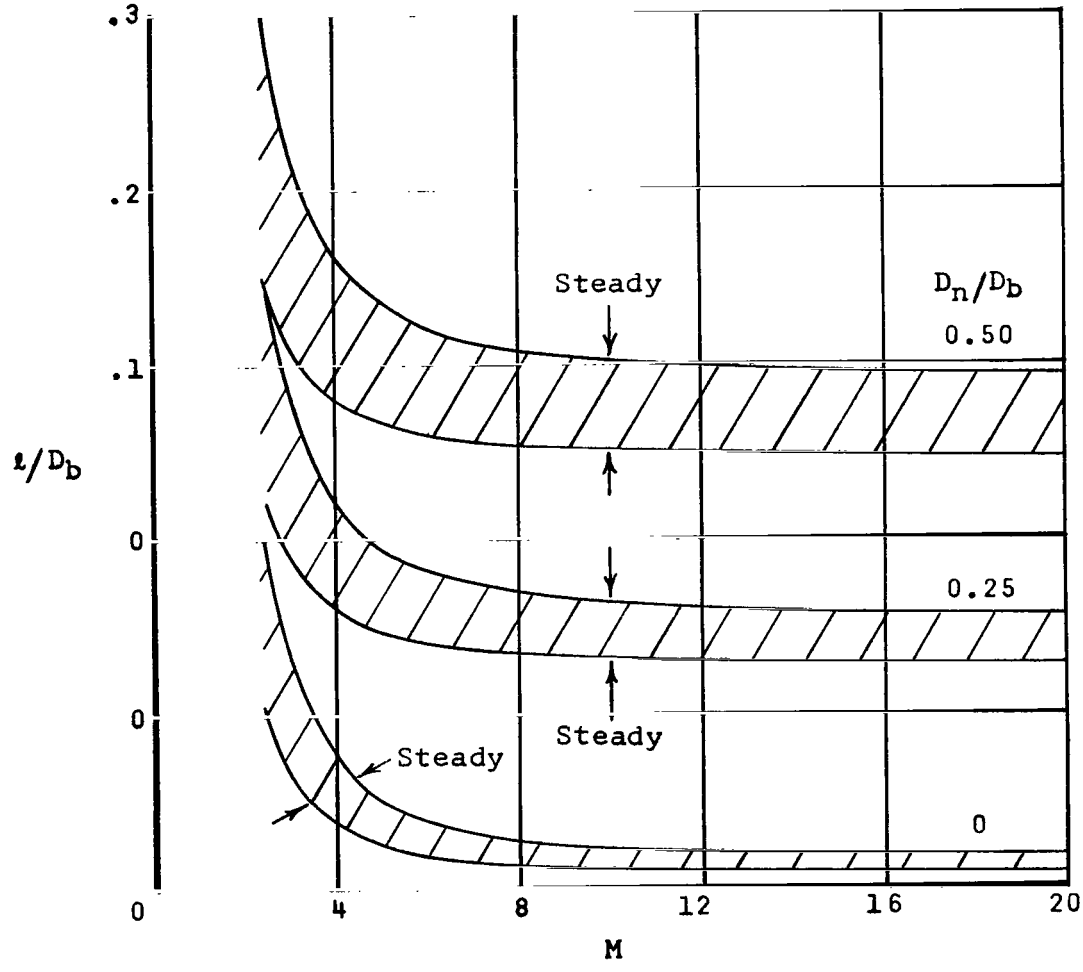

(b) Steady attached flow. $1.1 \leq \ell/\delta \leq 2.2$.

Figure 9.- Spike-length requirements for steady flow. $\Phi = 60^{0}$.

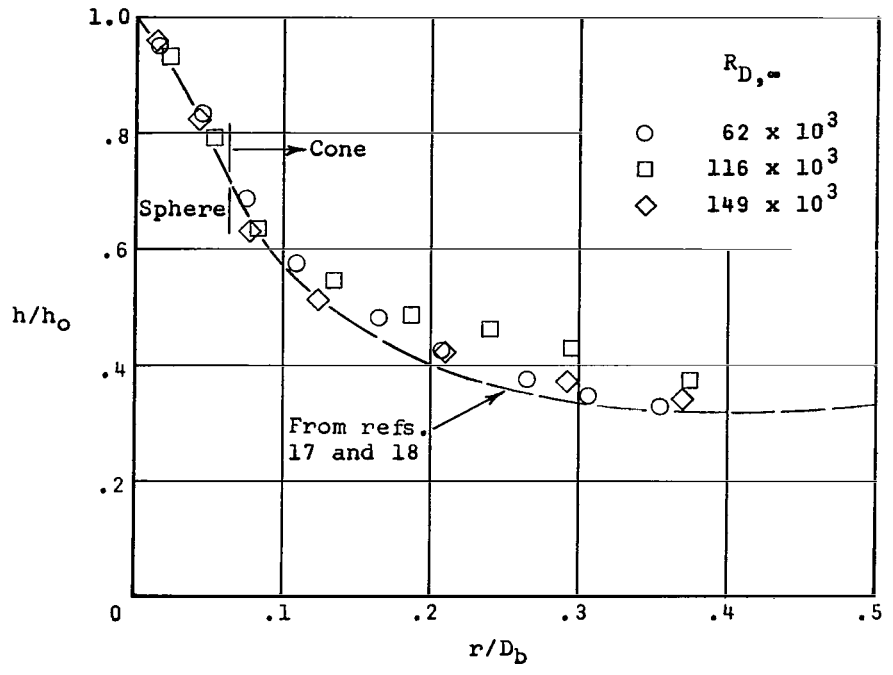

(a) $\frac{D_n}{D_b} = 0.25$.

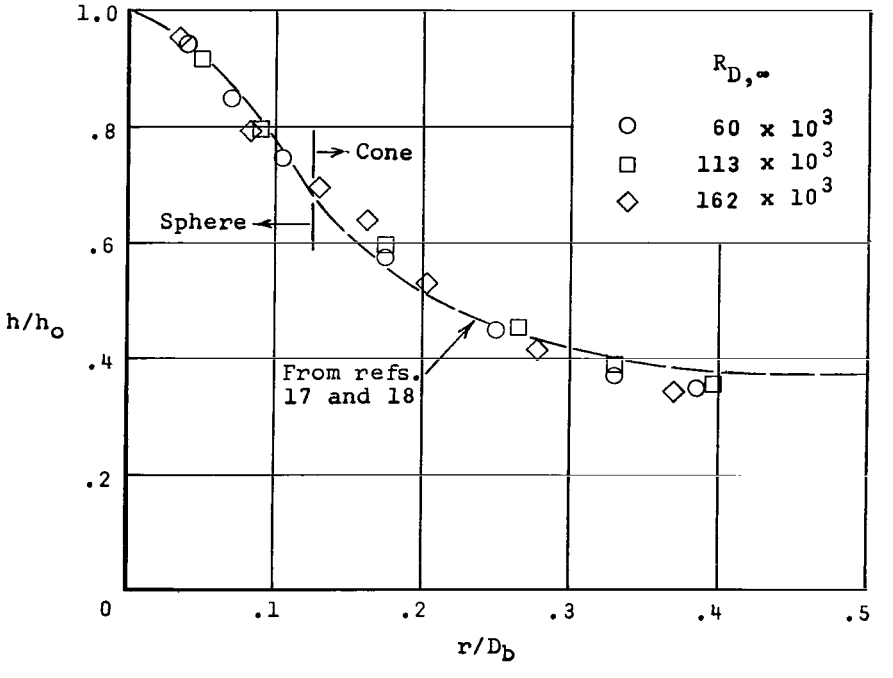

(b) $\frac{D_n}{D_b} = 0.50$.

Figure 10.- Effect of Reynolds number on unspiked model heat transfer. $\frac{l}{D_b} = 0.0$; $\Phi = 60^0$.

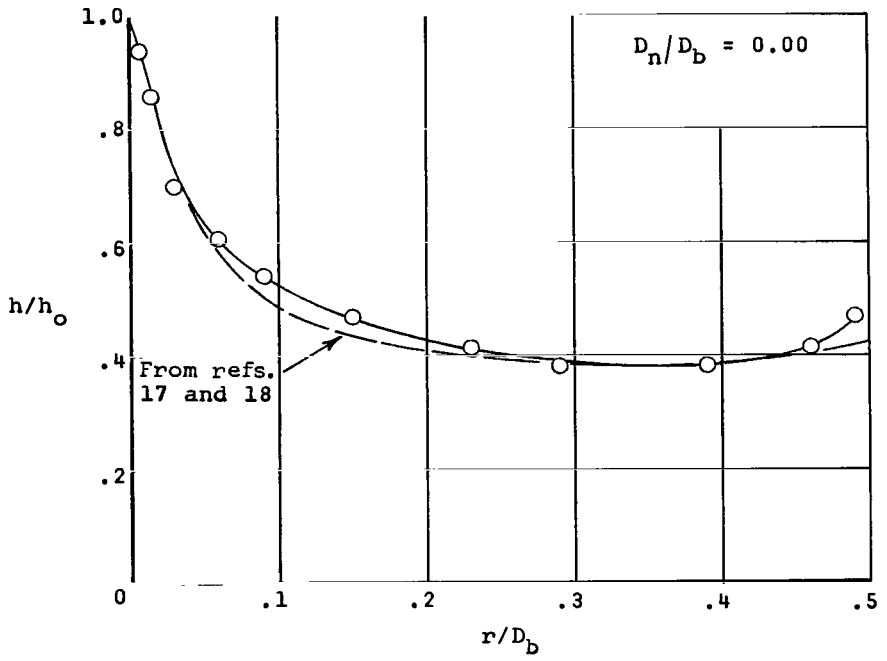

(a) $\Phi = 70^0$.

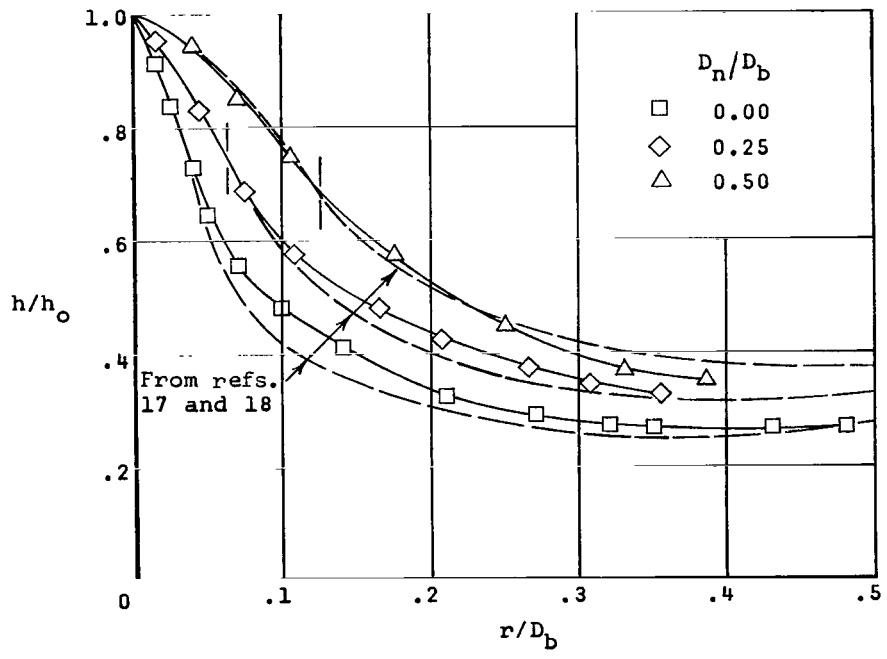

(b) $\Phi = 60^0$.

Figure 11.- Unspiked model heat transfer. $\frac{l}{D_b} = 0.00$; $R_{D,\infty} \approx 6 \times 10^4$.

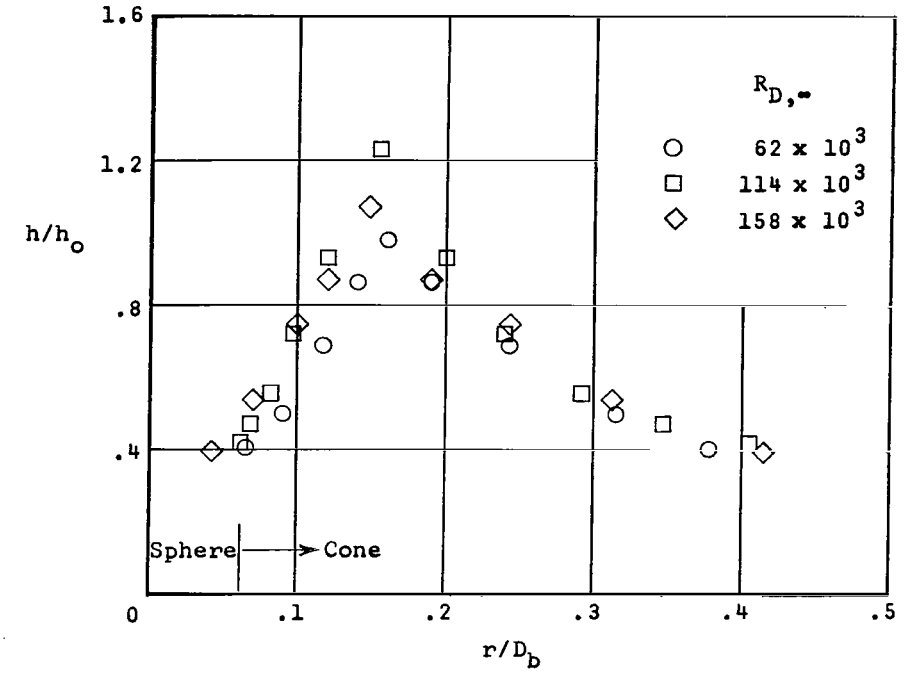

(a) $\frac{D_n}{D_b} = 0.25$.

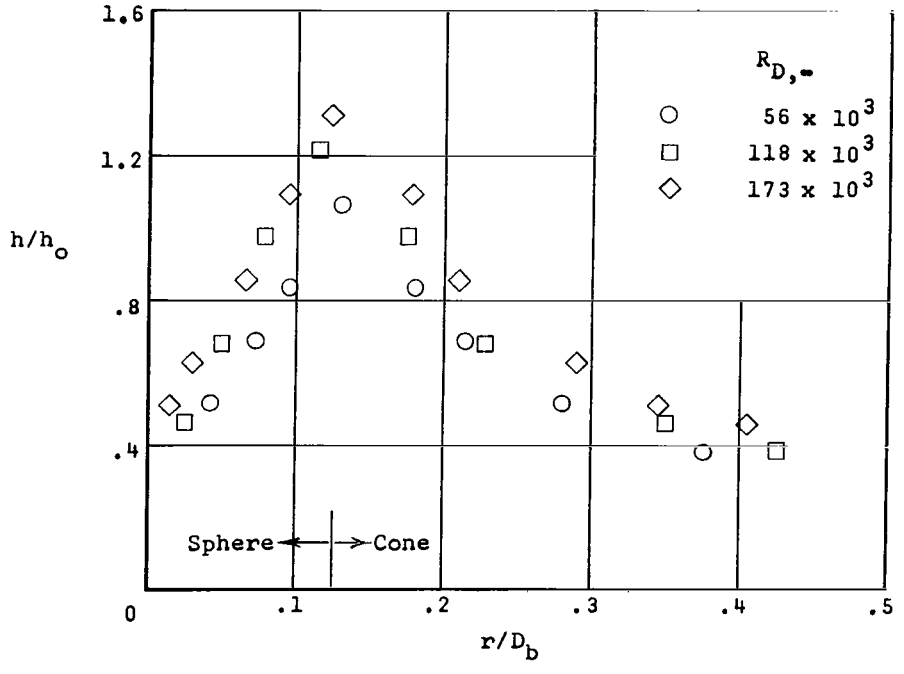

(b) $\frac{D_n}{D_b} = 0.50$.

Figure 12.- Effect of Reynolds number on body heat transfer with a spike. $\frac{l}{D_b} = 0.0767$; $\Phi = 60^o$.

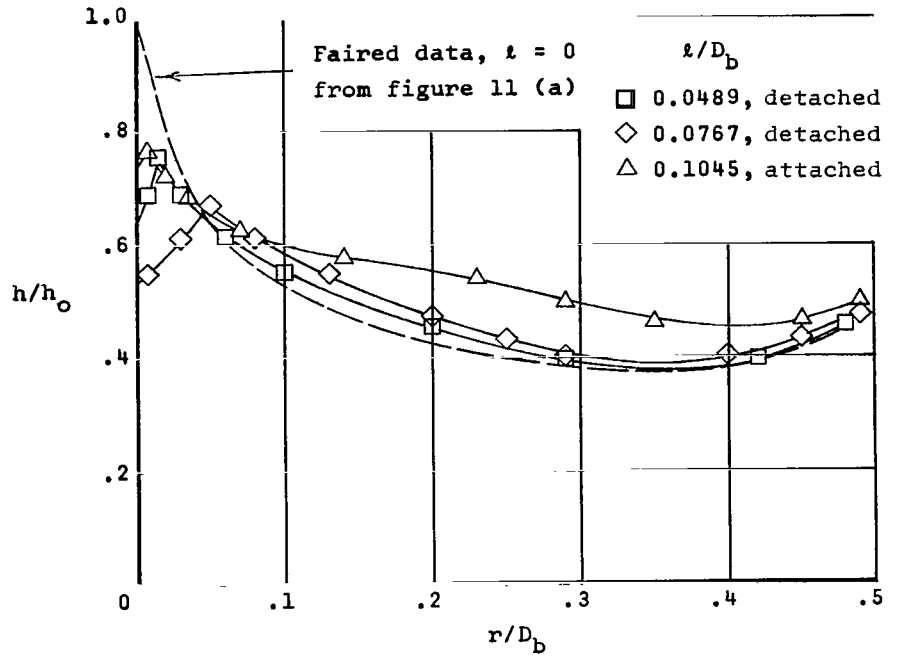

(a) $\Phi = 70^0$; $\frac{D_n}{D_b} = 0.$

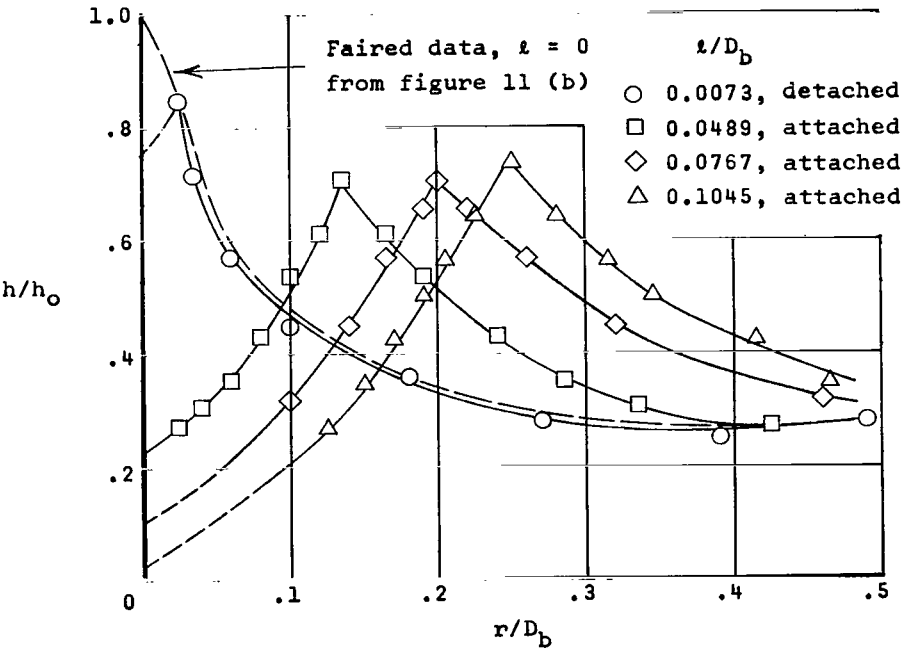

(b) $\Phi = 60^0$; $\frac{D_n}{D_b} = 0.$

Figure 13.- Effect of spike length on heat-transfer distribution. $R_{D,\infty} \approx 6 \times 10^4$.

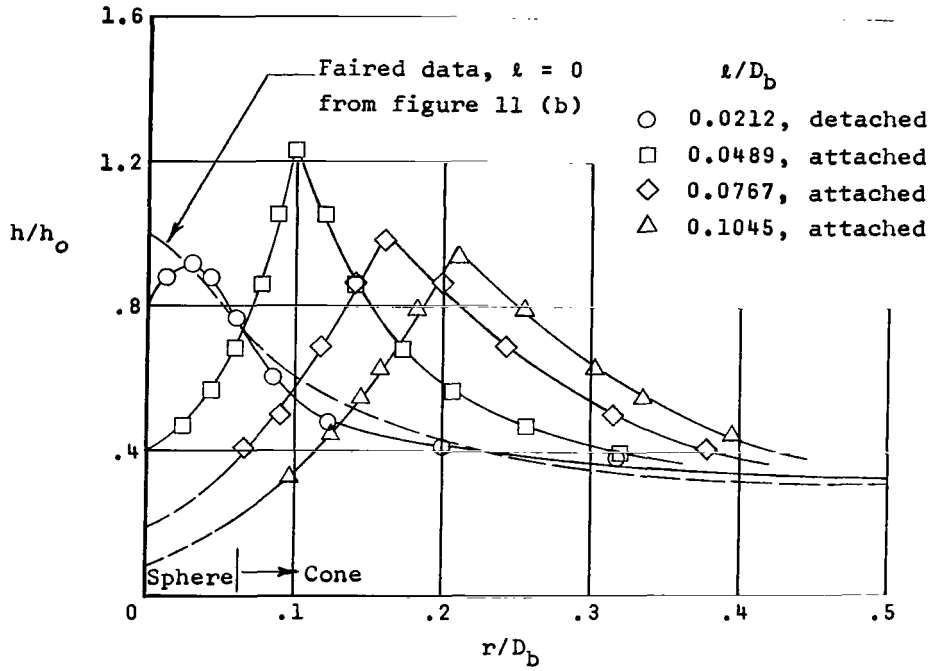

(c) $\Phi = 60^{\circ}$; $\frac{D_n}{D_b} = 0.25$.

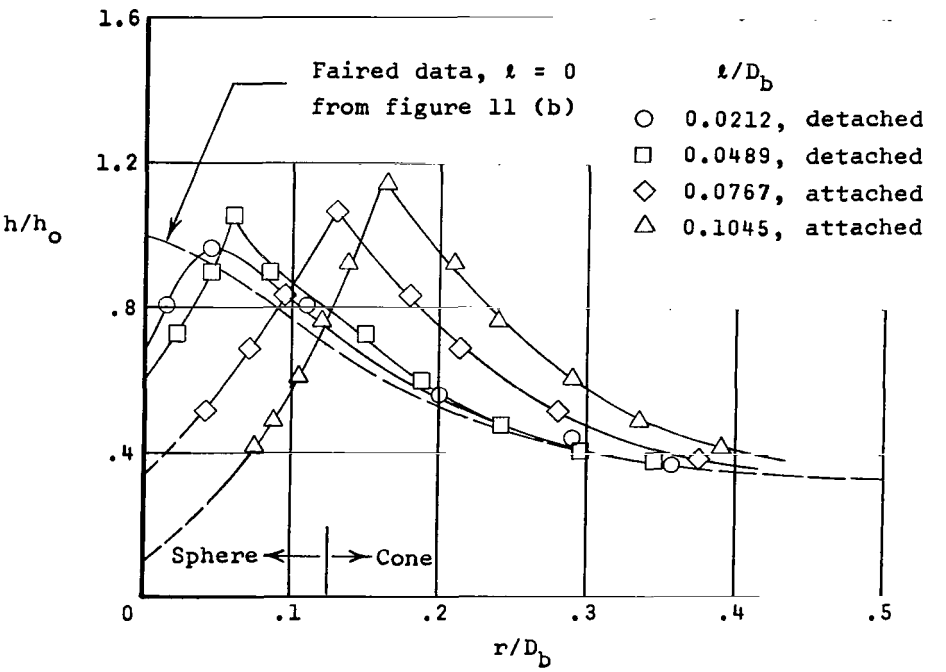

(d) $\Phi = 60^{\circ}$; $\frac{D_n}{D_b} = 0.50$.

Figure 13.- Concluded.

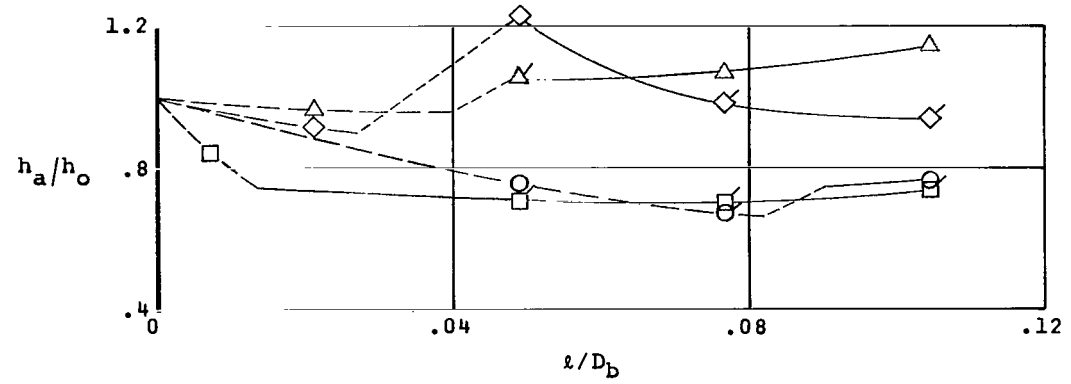

(a) Heating at flow attachment.

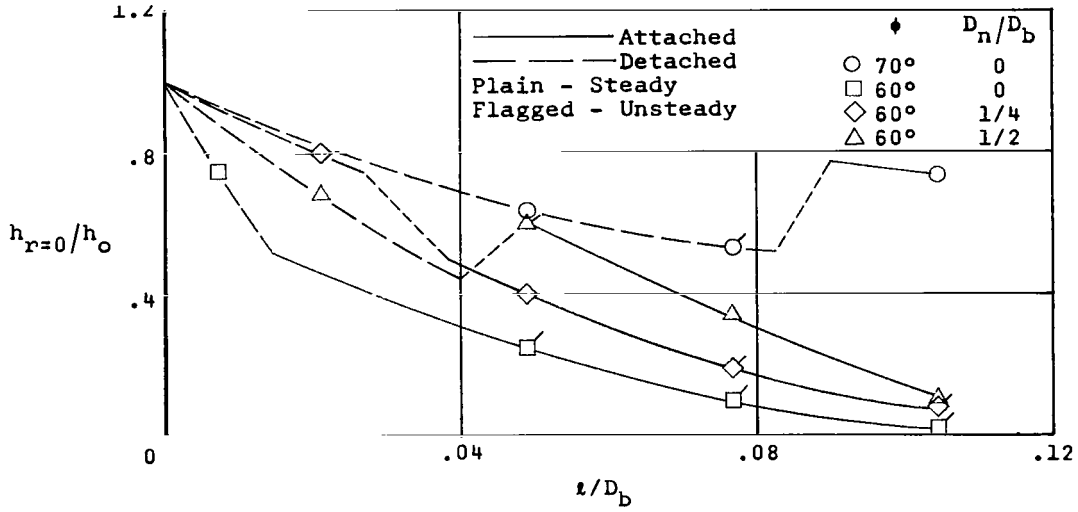

(b) Heating extrapolated to $r \approx 0$.

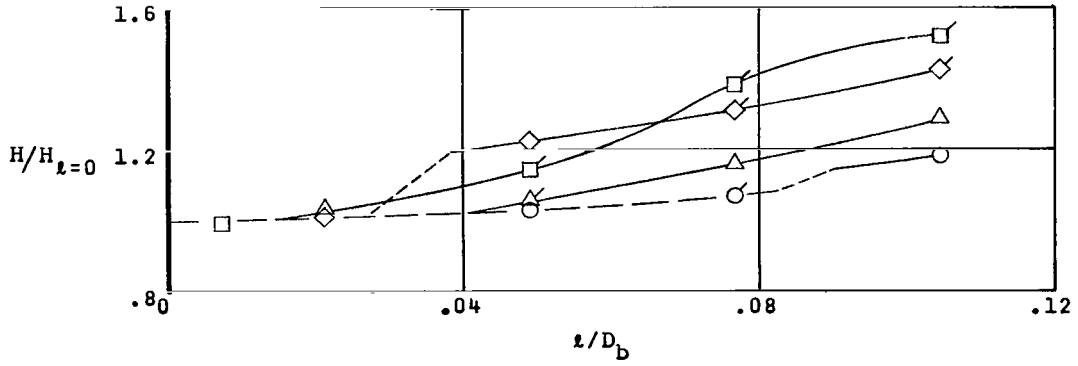

(c) Total integrated heating on body.

Figure 14.- Effects of spike length on body heating. $R_{D,\infty} \approx 6 \times 10^4$.

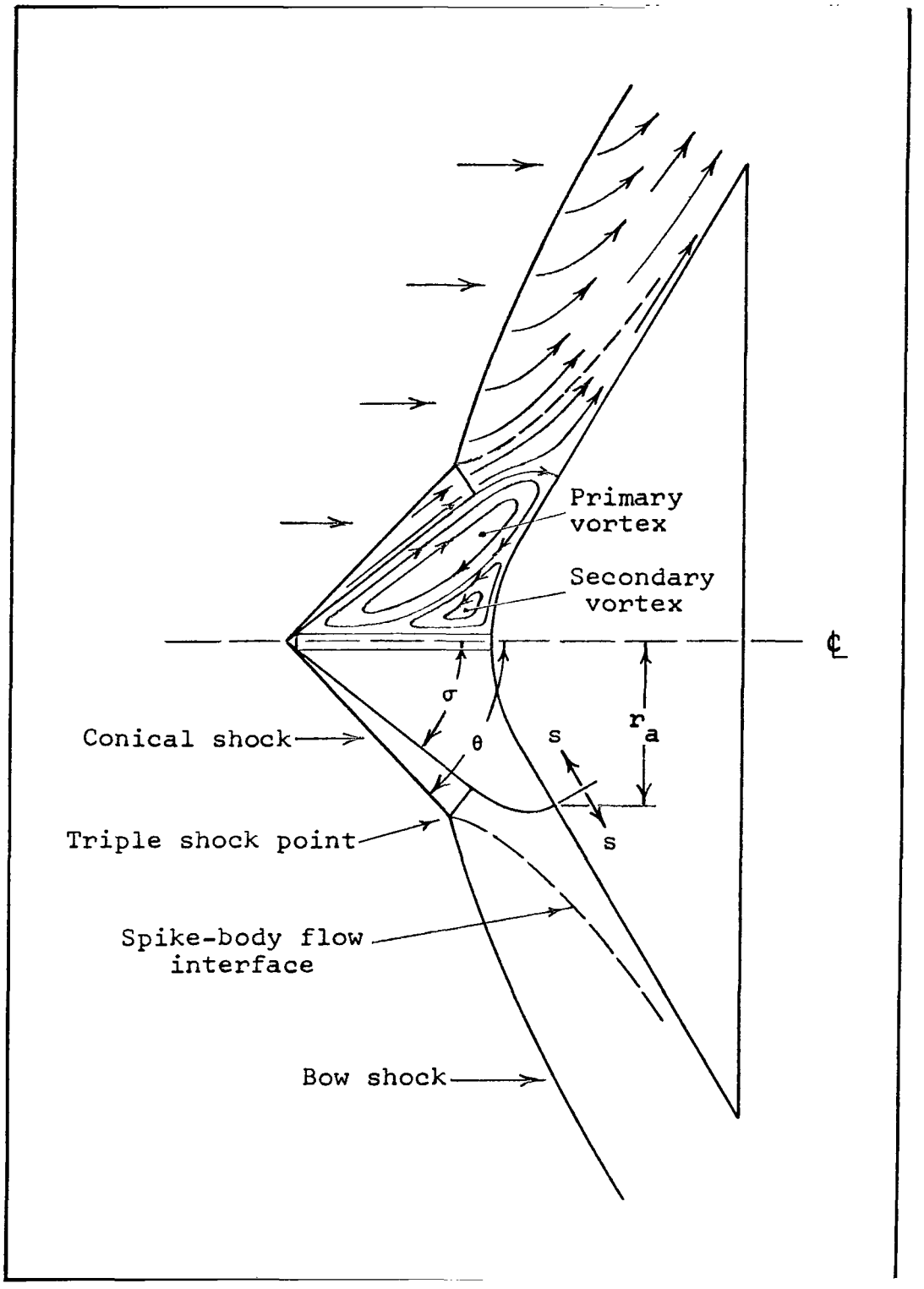

Figure 15.- Postulated flow model.

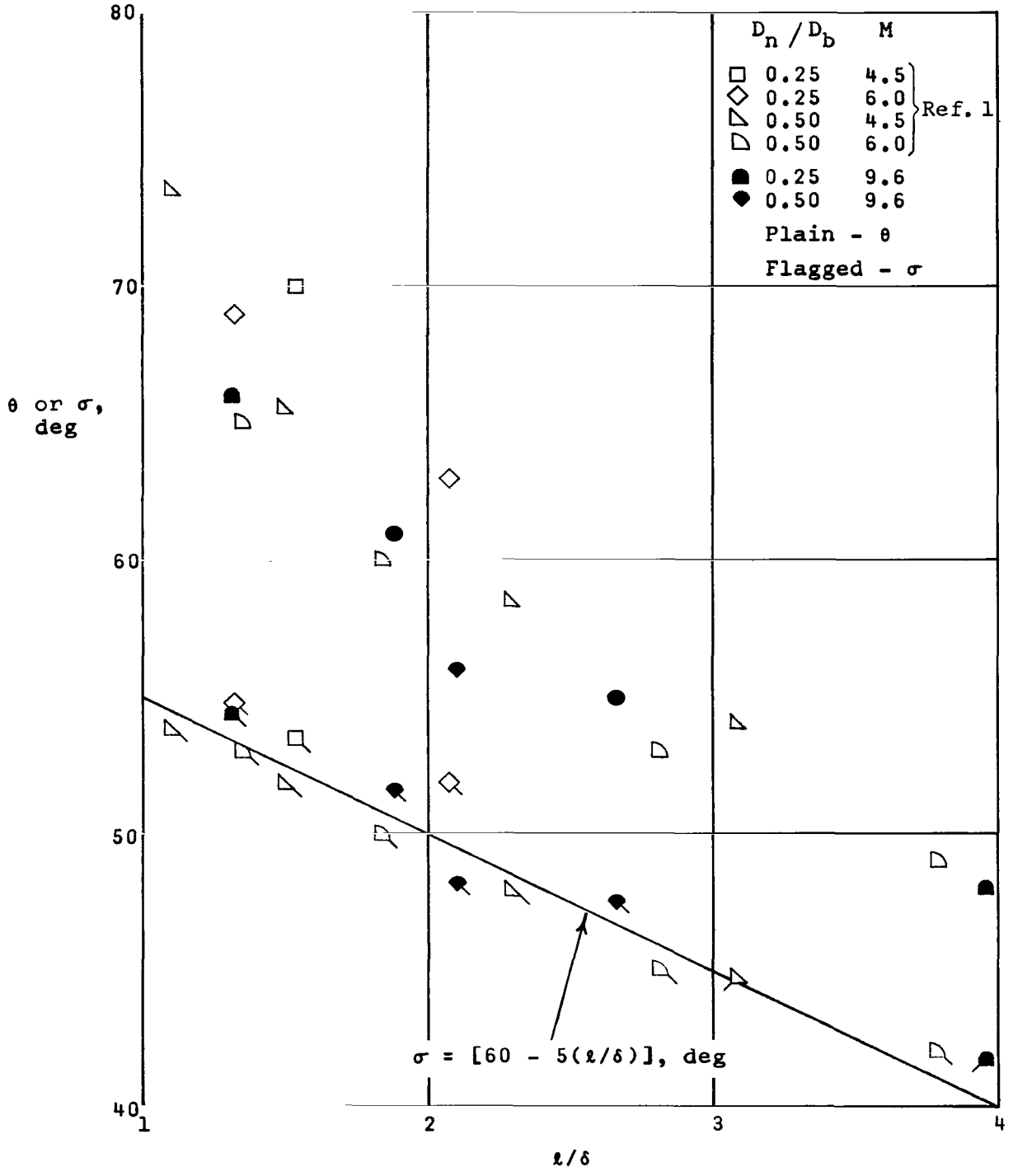

Figure 16.- Attached spike shock and equivalent cone angles. $\Phi = 60^{0}$.

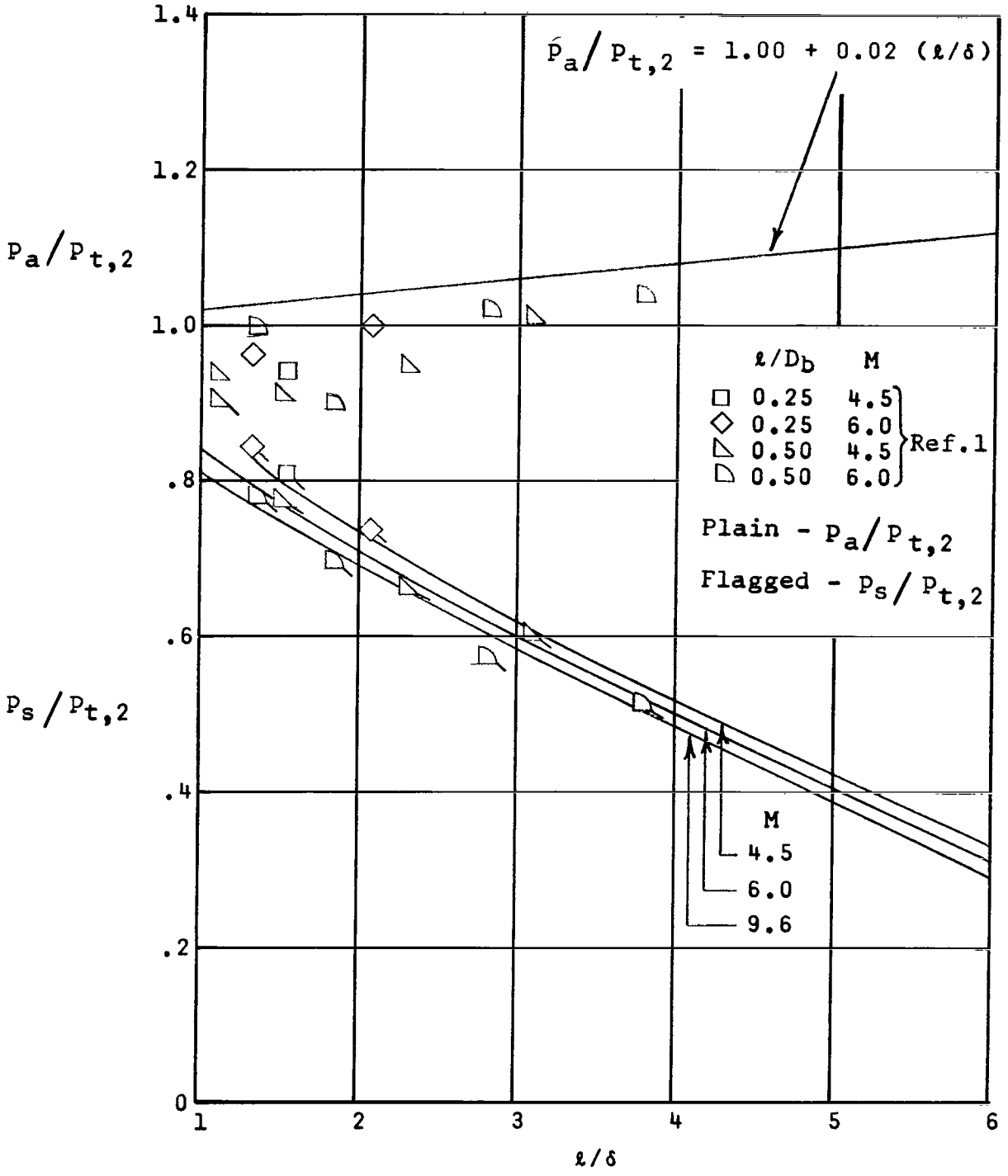

Figure 17.- Separation and attachment pressures. $\Phi = 60^{\circ}$.

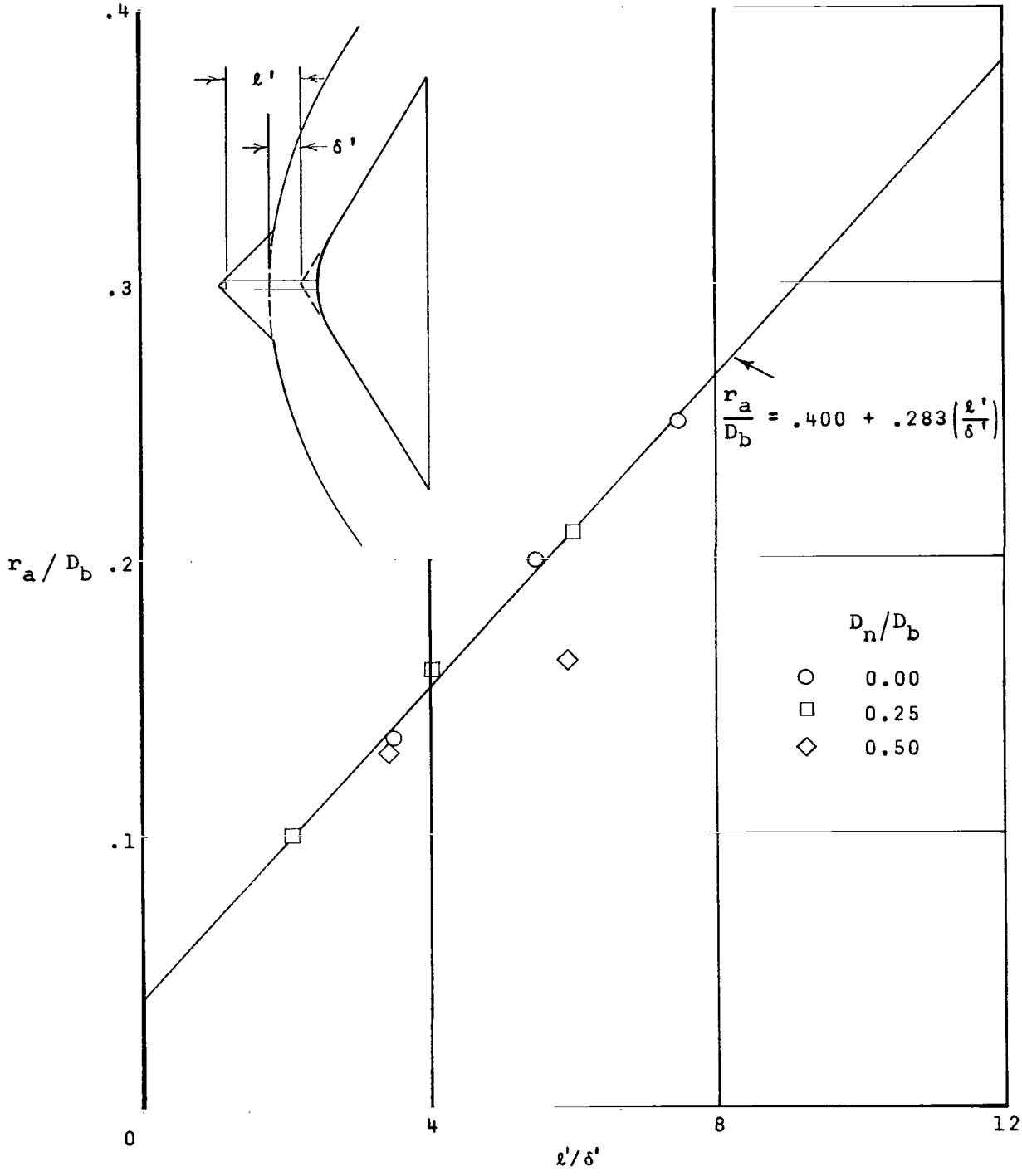

Figure 18.- Flow attachment point. $\Phi = 60^{\circ}$; $R_{D,\infty} \approx 6 \times 10^4$.

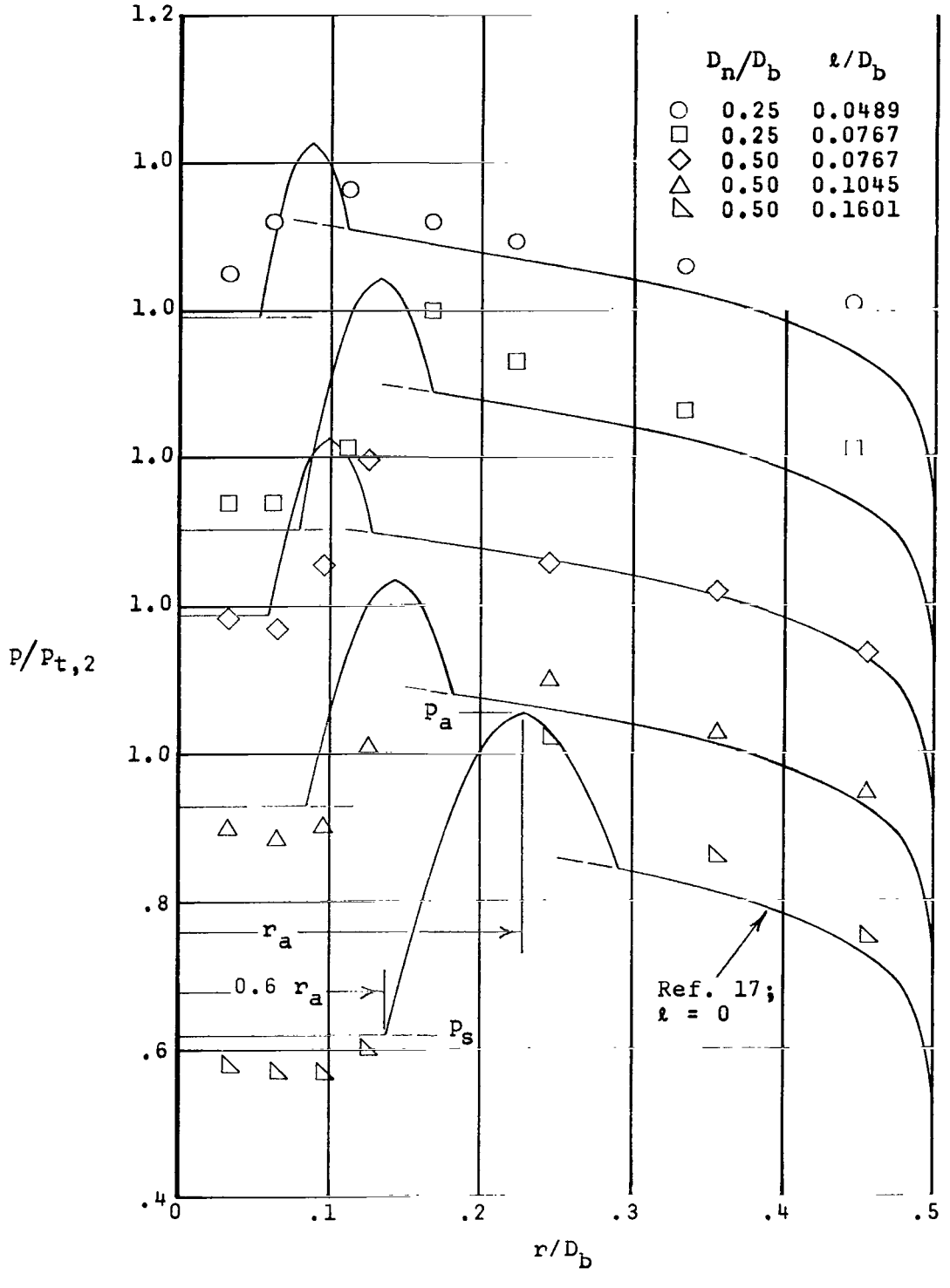

Figure 19.- Comparison of pressure data with predictions. M = 6.0, reference 1.

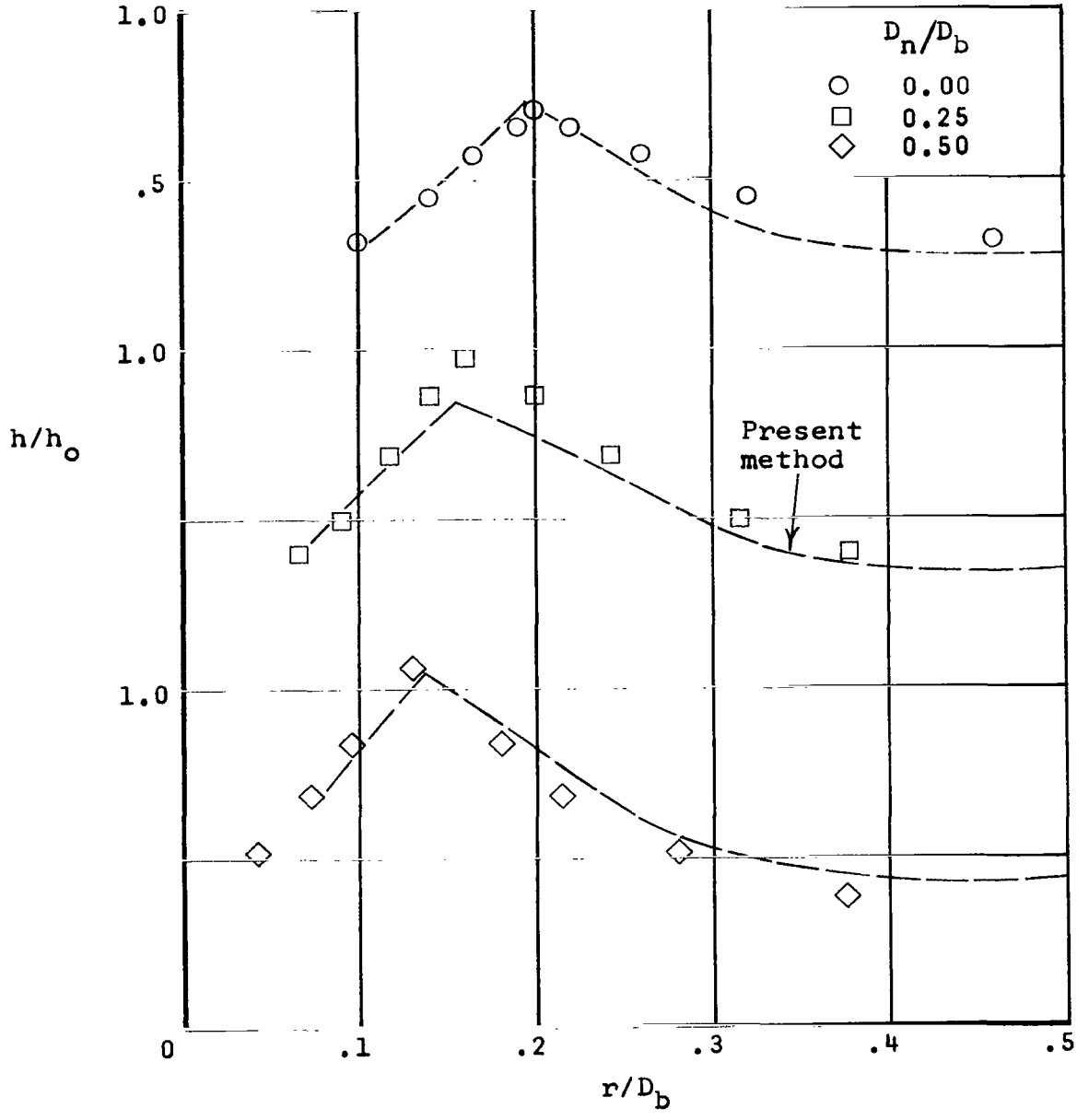

Figure 20.- Comparison of heat-transfer data with predictions. $\Phi = 60^0$; $\frac{l}{D_b} = 0.0767$; $R_{D,\infty} = 6 \times 10^4$; $M = 9.6$.

NATIONAL AERONAUTICS AND SPACE ADMINISTRATION
WASHINGTON, D. C. 20546

OFFICIAL BUSINESS

FIRST CLASS MAIL

POSTAGE AND FEES PAID
NATIONAL AERONAUTICS AND
SPACE ADMINISTRATION

POSTMASTER: If Undeliverable (Section 158 Postal Manual) Do Not Return

"The aeronautical and space activities of the United States shall be conducted so as to contribute . . . to the expansion of human knowledge of phenomena in the atmosphere and space. The Administration shall provide for the widest practicable and appropriate dissemination of information concerning its activities and the results thereof."

—NATIONAL AERONAUTICS AND SPACE ACT OF 1958

NASA SCIENTIFIC AND TECHNICAL PUBLICATIONS

TECHNICAL REPORTS: Scientific and technical information considered important, complete, and a lasting contribution to existing knowledge.

TECHNICAL NOTES: Information less broad in scope but nevertheless of importance as a contribution to existing knowledge.

TECHNICAL MEMORANDUMS: Information receiving limited distribution because of preliminary data, security classification, or other reasons.

CONTRACTOR REPORTS: Scientific and technical information generated under a NASA contract or grant and considered an important contribution to existing knowledge.

TECHNICAL TRANSLATIONS: Information published in a foreign language considered to merit NASA distribution in English.

SPECIAL PUBLICATIONS: Information derived from or of value to NASA activities. Publications include conference proceedings, monographs, data compilations, handbooks, sourcebooks, and special bibliographies.

TECHNOLOGY UTILIZATION PUBLICATIONS: Information on technology used by NASA that may be of particular interest in commercial and other non-aerospace applications. Publications include Tech Briefs, Technology Utilization Reports and Notes, and Technology Surveys.

Details on the availability of these publications may be obtained from:

SCIENTIFIC AND TECHNICAL INFORMATION DIVISION

NATIONAL AERONAUTICS AND SPACE ADMINISTRATION

Washington, D.C. 20546